Multiaxial Fatigue Analyses and Life Predictions Using Finite Element Method

By

Hicham El-Hage

A Thesis

Submitted to the Faculty of Graduate Studies and Research through
Mechanical, Automotive and Materials Engineering Program
In Partial Fulfillment of the requirements for the
Degree of Master of Applied Science at the
University of Windsor

Windsor, Ontario, Canada
2000

I hereby declare that I am the sole author of this document.

I authorize the University of Windsor to lend this document to other institutions or individuals for the purpose of scholarly research.

Hicham El-Hage

I further authorize the University of Windsor to reproduce the document by photocopying or by other means, in total or in part, at the request of other institution or individuals for the purpose of scholarly research.

Hicham El-Hage

ABSTRACT

In predicting the fatigue lives of structural or mechanical components, there are several multiaxial fatigue theories that can be used to evaluate the fatigue crack initiation. However, there exists a lack of agreements on which theory models the fatigue crack initiation most appropriately.

The purpose of this thesis is to evaluate the validity of most commonly used multiaxial fatigue criteria; specifically the maximum principal strain and the maximum shear strain criteria. Moreover, a new criterion based on strain energy density is proposed and evaluated for elastic and elastic-plastic damage scenarios. The best criterion, identified through comparative analyses, is used to evaluate the fatigue lives of two connecting rods supplied by an automotive company.

Three-dimensional finite element analysis is performed on the SAE notch shaft, which is used as a test component to evaluate the validity of the existing and proposed multiaxial fatigue damage criteria. Elastic and elastic-plastic stress-strain responses are then used to obtain the required damage parameters that are eventually used to predict the fatigue lives.

The two existing multiaxial fatigue theories, maximum principal strain and maximum shear strain, seem to differ in predicting the fatigue lives of the SAE notch shaft. The proposed criteria, elastic and elastic-plastic strain energy density; also differ in predicting the fatigue lives of the SAE notch shaft. However, the maximum principal strain and the elastic-plastic strain energy density approaches seem to deliver the best results when they are compared to the reported experimental results. These two approaches predict the fatigue lives within ranges that differ from each other. However the difference among these ranges depends upon whether the fatigue lives are evaluated for low-cycle or high-cycle fatigue regions. It is noticeable that the maximum principal strain criterion delivers

better results than the elastic-plastic strain energy density approach in low-cycle fatigue regions. However, the latter delivers much better results in high-cycle fatigue regions and its ranges in low-cycle fatigue regions do not differ greatly from the maximum principal strain ranges. The maximum shear strain criterion predicts the fatigue lives conservatively. In other word, its predicted fatigue lives are much less than the experimental fatigue lives that are reported in the literature. Also, analyses have shown that the elastic strain energy density approach delivers the fatigue lives excessively. In other word, it overestimates the fatigue lives. However this approach delivers the best results in high-cycle fatigue regions where plastic strain is a small potion of the total strain.

DEDICATION

TO MY WIFE IMAN, MY SON BASSAM

AND MY DAUGHTER NOUR

ACKNOWLEDGEMENTS

The author wishes to express his deep gratitude to his advisor, ***Dr. Sudip Bhattacharjee***, for his support, guidance, effort and patience throughout the course of this research. His supervision is deeply appreciated.

Financial assistance and scholarships received from the University of Windsor and the Natural Sciences and Engineering Research Council of Canada are thankfully acknowledged.

The author also wishes to thank Mascotech for providing information regarding the properties and geometries of automotive connecting rods.

TABLE OF CONTENTS

LIST OF FIGURES

LIST OF TABLES

LIST OF SYMBOLS

A	amplitude ratio
A_f	area at fracture
A_0	original area
B	bending moment
b	fatigue strength exponent
c	fatigue ductility exponent
E	Young's modulus
e_{ij}	local elastic strain tensor
K	strength coefficient
K'	cyclic strength coefficient
K_I	stress intensity factor
N	number of cycles
n	strain hardening exponent
n'	cyclic hardening exponent
P_f	load at fracture
RA	reduction in area
r	radial coordinate in the polar coordinate system
r_p	radius of plastic zone
SAE	Society of Automotive Engineerings
S_{ij}	local elastic stress tensor
SR	stress ratio
T	torque
U	total strain energy density
U_e	elastic strain energy density
U_p	plastic strain energy density
U_s	strain energy density due to local elastic stress-strain field
U_σ	strain energy density due to local elastic-plastic stress-strain field

γ	shear strain
γ_{max}	maximum shear strain
ε	strain
$\varepsilon_1, \varepsilon_2, \varepsilon_3$	principal strains
ε_e	elastic strain contribution
$\varepsilon_{f'}$	fatigue ductility coefficient
ε_{ij}	local elastic-plastic strain tensor
ε_p	plastic strain contribution
ε_t	total strain
$d\varepsilon$	strain increment
$\Delta\varepsilon$	strain range
$\Delta\varepsilon_e$	elastic strain range
$\Delta\varepsilon_p$	plastic strain range
ν	Poisson's ratio
σ	stress
σ_a	alternating stress
$d\sigma$	stress increment
$\sigma_{f'}$	fatigue strength coefficient
σ_{ij}	local elastic-plastic regime stress tensor
σ_u	ultimate stress
$\sigma_x, \sigma_y, \sigma_z$	local stress components in elastic-plastic plane stress condition; Cartesian coordinates
$\Delta\sigma$	stress range

Chapter 1

Introduction

1.1 General

Static or quasistatic loading is rarely observed in modern engineering practice, making it essential to the engineer to direct himself/herself to implications of repeated loads, fluctuating loads, and rapidly applied loads. By far, the majority of engineering design projects involves machine parts subjected to fluctuating or cyclic loads. Such loading induces fluctuating or cyclic stresses that often result in failure by fatigue. The most difficult aspect of fatigue is to detect the progressive changes in material properties that occur during cyclic stressing, and the failure may therefore occur with no apparent warning. Also, periods of rest, with the fatigue stress removed, do not lead to any measurable healing or recovery from the effects of the prior cyclic stressing. Thus the damage done during the fatigue process is cumulative, and generally unrecoverable.

Fatigue failure investigations over the years have led to the observation that the fatigue process actually embraces two domains of cyclic stressing or straining that are significantly different in character, and in each of which failure is probably produced by different physical mechanisms. One domain of cyclic loading is that for which plastic strain occurs during each cycle. This domain is associated with high loads and short lives, or low-cycle fatigue (LCF). The other domain of cyclic loading is that for which the strain cycles are largely confined to elastic range. This domain is associated with lower loads and long lives, or high cycle fatigue (HCF). Low-cycle fatigue is typically associated with cycle lives from one to about 10^4 or 10^5 cycles, and high-cycle fatigue for lives greater than about 10^4 or 10^5 cycles.

In recent years, it has been recognized that the fatigue failure process involves three phases. A crack initiation phase occurs first, followed by crack propagation phase; finally, when the crack reaches a critical size, the final phase of unstable rapid crack growth to fracture completes the failure process. The modeling of these phases has been

under intense scrutiny, but the models have not yet been developed in a coordinated way to provide widely accepted engineering design tools.

Nevertheless, great progress has been made in the crack propagation modeling and in modeling the final fracture phase. Although progress has been much slower in modeling the crack initiation phase, the most promising approach to the prediction of crack initiation seems to be the local stress-strain approach. The basic premise of the local stress-strain approach is that the local fatigue response of the material at critical point, that is, the site of crack initiation, is analogous to the fatigue response of a small, smooth specimen subjected to the same cyclic strains and stresses. The cyclic stress-strain response of the critical material may be determined from the characterizing smooth specimen through appropriate laboratory testing.

To properly perform such laboratory tests, the local cyclic stress-strain history at the critical point in the structure must be determined, either by analytical or experimental means. Thus valid stress analysis procedures, finite element modeling, or experimental strain measurements are necessary, and the ability to properly account for plastic behavior must be included. In performing smooth specimen tests of this type, it must be recognized that the phenomena of cyclic hardening, cyclic softening, and cycle-dependent stress relaxation, as well as sequential loading effects and residual stress effects that may be experienced by the specimen as it accumulates fatigue damage are presumed to be the same as at the critical point of the structure member being simulated.

Since, including all these factors in a test is inconvenient, inaccurate and expensive, the use of finite element method has become a powerful tool to calculate the cyclic stress-strain response of any structure or mechanical component. The finite element method is especially used in the ground vehicle industry where discontinuities of the geometry such as notches and holes produce difficulties to calculate the local cyclic stresses and strains, which are essential to predict the fatigue life of any structure or component.

1.2 Research Objectives

The objective of this research is to investigate the validity of commonly used multiaxial fatigue life predictions criteria. Specifically, the maximum principal strain and the maximum shear strain. These criteria are used to predict the fatigue crack initiation of the total life. Moreover, unified strain energy density based methodology that can be used for high-cycle and low-cycle fatigue life predictions will be developed.

Based on the best fatigue life prediction criterion, fatigue life assessment of two connecting rods will be carried out. It is important to note that the analysis is performed for constant amplitude load cycles only.

1.3 Thesis Outline

Literature review is presented in Chapter 2 of this thesis. It includes discussions of the existing multiaxial fatigue theories, stress, strain, and fracture mechanics approaches of fatigue life predictions.

In Chapter 3, criteria for fatigue life predictions and overview of multiaxial fatigue theories are presented, followed by analysis of the Society of Automotive Engineerings (SAE) test shaft. Furthermore details on the finite element techniques used in the analysis are also presented in this chapter. Moreover, fatigue life predictions by the existing multiaxial fatigue theories and the proposed strain energy density approaches are also investigated in this chapter. The fatigue life predictions are compared to experimental fatigue lives that exist in the literature [12], and then comments and general conclusions of the different fatigue lives criteria are made in this chapter as well.

Chapter 4, fatigue life predictions of connecting rods, is an industrial application based on the best criterion that is obtained from the previous analysis. This chapter includes description of the problem, finite element analysis, and fatigue life predictions of two

different connecting rods. A recommendation to Mascotech, an automotive company, is also included in this chapter.

In Chapter 5, Summary, conclusions and recommendations for future research are presented.

Chapter 2
Literature Review

2.1 Introduction

Methodology to predict fatigue crack initiation is divided into two principal steps: (i) calculation of local stresses and strains, and (ii) prediction of fatigue lives from calculated stress-strain responses.

2.2 Calculation of local stress-strain field

Almost all machine components and structural members contain some form of geometrical or microstructural discontinuities. These discontinuities, or stress concentrations, often result in maximum local stresses, at the discontinuities, which are many times greater than the nominal stress of the member. Moreover, in many applications, components are subjected to complicated states of stress and strain. Complex stress states, in which the three principal stresses are nonproportional or whose directions change during a loading cycle, very often occur at geometric discontinuities such as notches or joint connections. Fatigue under these conditions, termed multiaxial fatigue, is an important design consideration for reliable operation and optimization of many engineering components.

Traditionally, the two existing fatigue life prediction theories are used on local stresses and strains, which are calculated, by using Neuber's rule. However, the scope of using Neuber's rule is limited to simple geometric shapes only. Moreover, it is difficult to account for plastic strain by using Neuber's rule.

Finite element technique appears to be a powerful tool to predict local stress-strain response in a complex system that is subjected to complex loading. Moreover, the finite element technique is widely used in the automotive industry, especially for noise, vibration, and harshness NVH and crash performance verification of vehicle design. It is,

therefore, consistent to use the same modeling technique for fatigue durability assessment of the structural parts as well.

2.3 Fatigue life prediction

The fatigue life is often related to strain amplitude as shown in Fig. 2.1 [13]. To explain the graph, we first define the following terms:

Fatigue ductility coefficient $\varepsilon_f^{'}$ is the true strain corresponding to fracture in one reversal (point A in Figure 2.2). The plastic-strain begins at this point in Fig. 2.1.

Fatigue strength coefficient $\sigma_f^{'}$ is the true stress corresponding to fracture in one reversal (point A in Fig. 2.2) [14].

Fatigue ductility exponent c is the slope of the plastic-strain line in Fig. 2.1 and is the power to which the life *2N* must be raised to be proportional to the plastic-strain amplitude

Fatigue strength exponent b is the slope of the elastic-strain line, and is the power to which the life *2N* must be raised to be proportional to the true-stress amplitude.

From Fig. 2.1 , it is noted that the total strain is the sum of the elastic and plastic components. Therefore the total strain amplitude is

$$\frac{\Delta\varepsilon}{2} = \frac{\Delta\varepsilon_e}{2} + \frac{\Delta\varepsilon_p}{2} \qquad (2.1)$$

The equation of the plastic-strain line (Fig. 2.1) is

$$\frac{\Delta\varepsilon_p}{2} = \varepsilon_f^{'}(2N)^c \qquad (2.2)$$

The equation of the elastic-strain line is

$$\frac{\Delta\varepsilon_e}{2} = \frac{\sigma_f^{'}}{E}(2N)^b \qquad (2.3)$$

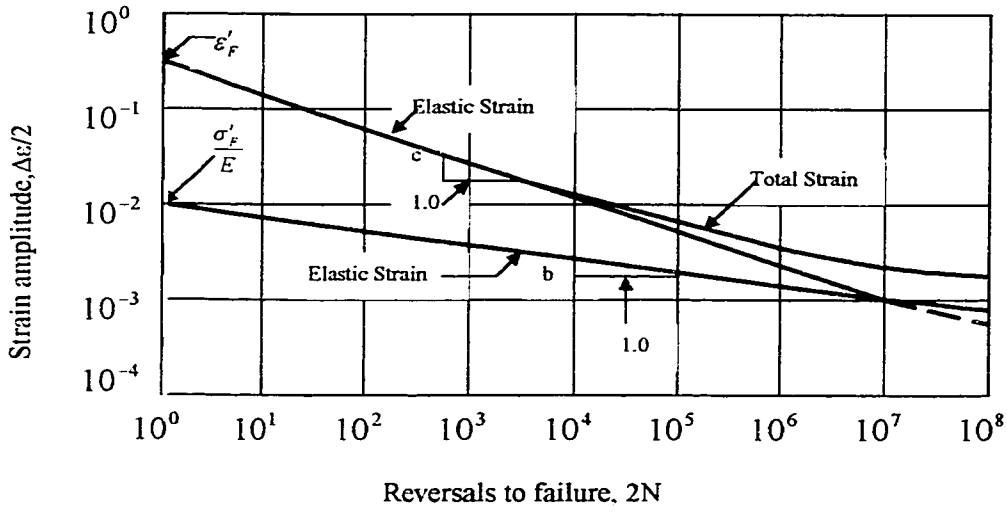

Figure 2.1 A log-log plot showing that the fatigue life is related to the true-strain amplitude [13].

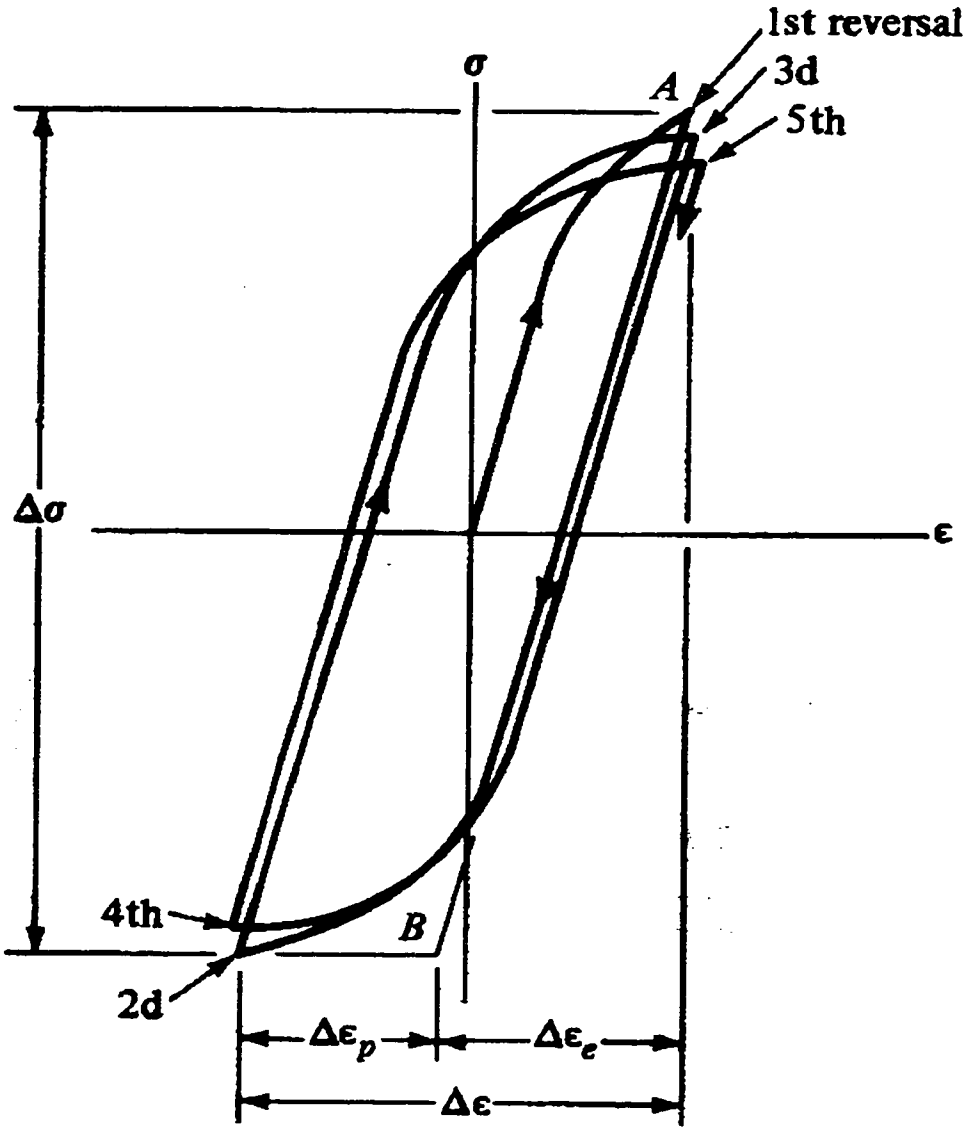

Figure 2.2 True stress-strain hysteresis loops [13].

Therefore, from Eq. 2.1, we have the total-strain amplitude, known as Manson-Coffin equation

$$\frac{\Delta \varepsilon}{2} = \frac{\sigma_f'}{E}(2N)^b + \varepsilon_f'(2N)^c \qquad (2.4)$$

The Manson-Coffin equation relates the fatigue life to strain amplitude. Having the stress and strain parameters at hand, one can calculate the fatigue life using the strain amplitude at the critical location of structural member. The basic Manson- Coffin equation has been used with different measures of the strain response. Two most common strain criteria, used for fatigue life calculations, are reviewed in the following sections.

2.3.1 Maximum Principal strain criterion

This criterion proposes that fatigue cracks initiate on planes, which experience the largest amplitude of principal strain. For uniaxial stress, the maximum principal strain is the axial strain in the direction of the applied stress. Replacing the axial strain in Eq. 2.4 by the maximum principal strain, which is obtained from three dimensional finite element analysis, will enable us to predict the fatigue life of three-dimensional case [6].

$$\frac{\Delta \varepsilon_1}{2} = \frac{\sigma_f'}{E}(2N)^b + \varepsilon_f'(2N)^c \qquad (2.5)$$

2.3.2 Maximum shear strain criterion

It has been observed that fatigue cracks often initiate on shear planes. The maximum shear strain criterion proposes that cracks will initiate on planes, which experience the maximum shear strain amplitude.

If $\varepsilon_1 \geq \varepsilon_2 \geq \varepsilon_3$, crack initiation takes place on the plane at 45^0 to the plane perpendicular ε_1 Fig. 2.3.

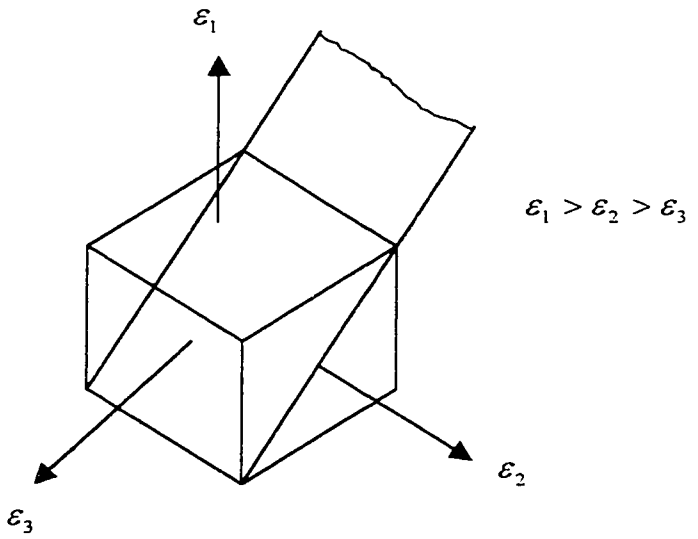

Figure 2.3 Plane of maximum shear strain [6].

The maximum shear strain can be calculated from the principal strains using Mohr's circle (Fig. 2.4), where the maximum shear strain is given by

$$\frac{\gamma_{max}}{2} = \frac{\varepsilon_1 - \varepsilon_3}{2} \tag{2.6}$$

An equation based on the maximum shear strain should give the same calculated endurance for a uniaxial stress condition as the uniaxial strain-life Eq. 2.5. For uniaxial stress, with an axial strain ε_1, and the principal strains $\varepsilon_2 = \varepsilon_3 = -\nu\varepsilon_1$, we have from Eq 2.6:

$$\gamma_{max} = \varepsilon_1 - \varepsilon_2 = \varepsilon_1 - (\nu\varepsilon_1) = (1+\nu)\varepsilon_1$$

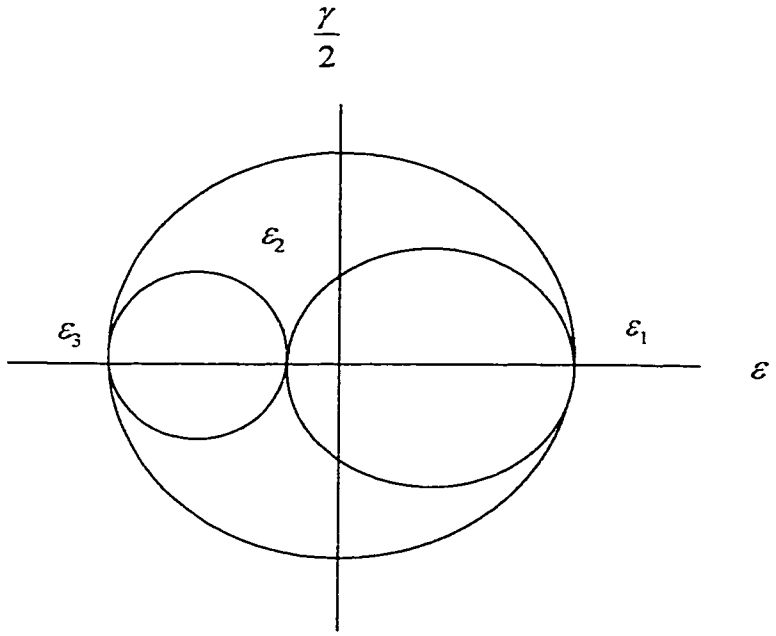

Figure 2.4 Mohr's strain circle [6].

For elastic strains, Poisson's ratio ν is approximately 0.3 for steel, so that

$$\gamma_{max} = 1.3\varepsilon_1$$

As the shear strain amplitude is 1.3 times the direct strain amplitude, the elastic part of Eq. 2.4, that is

$$\frac{\Delta\varepsilon}{2} = \frac{\sigma_f'}{E}(2N)^b$$

must be multiplied by 1.3, giving

$$\frac{\Delta\gamma_{max}}{2} = 1.3\frac{\sigma_f'}{E}(2N)^b$$

For purely plastic strains, ν=0.5, so that

$$\gamma_{max} = 1.5\varepsilon_1$$

and so the plastic part of the equation (2.4) becomes

$$\frac{\Delta\gamma_{max}}{2} = 1.5\varepsilon_f'(2N)^c$$

The uniaxial strain-life equation (2.4), expressed in terms of γ_{max}, is therefore

$$\frac{\Delta\gamma_{max}}{2} = 1.3\frac{\sigma_f'}{E}(2N)^b + 1.5\varepsilon_f'(2N)^c \qquad (2.7)$$

2.4 Stress-life approach

2.4.1 Introduction

The stress-life, *S-N*, method was the first approach used in attempt to comprehend and quantify metal fatigue. It was the standard fatigue design method for almost a century. The *S-N* approach is still widely used in design applications where the applied stress is primarily within the elastic range of the material and the resultant lives are long. The stress-life method does not work well in low-cycle fatigue applications where the applied strains have a significant plastic component.

2.4.2 Fatigue loading

Faced with the design of a fatigue sensitive element in a machine or structure, a designer is critically interested in the fatigue response of engineering materials to various loadings that might occur throughout the design life of the machine under consideration. That is, he/she is interested in the effects of various loading spectra and associated stress spectra, which will in general be a function of the design configuration and the operational use of the machine.

Perhaps the simplest fatigue stress spectrum to which an element may be subjected is a zero-mean sinusoidal stress-time pattern of constant amplitude and fixed frequency, applied for a specific number of cycles. Such a stress-time pattern, often referred to as completely reversed cyclic stress, is illustrated in Fig. 2.5(a). Utilizing the sketch of Fig. 2.5, we can conveniently define several useful terms and symbols; these include:

σ_{max} is the maximum stress in the cycle

σ_{min} is the minimum stress in the cycle

σ_m is the mean stress ($\frac{\sigma_{max} + \sigma_{min}}{2}$)

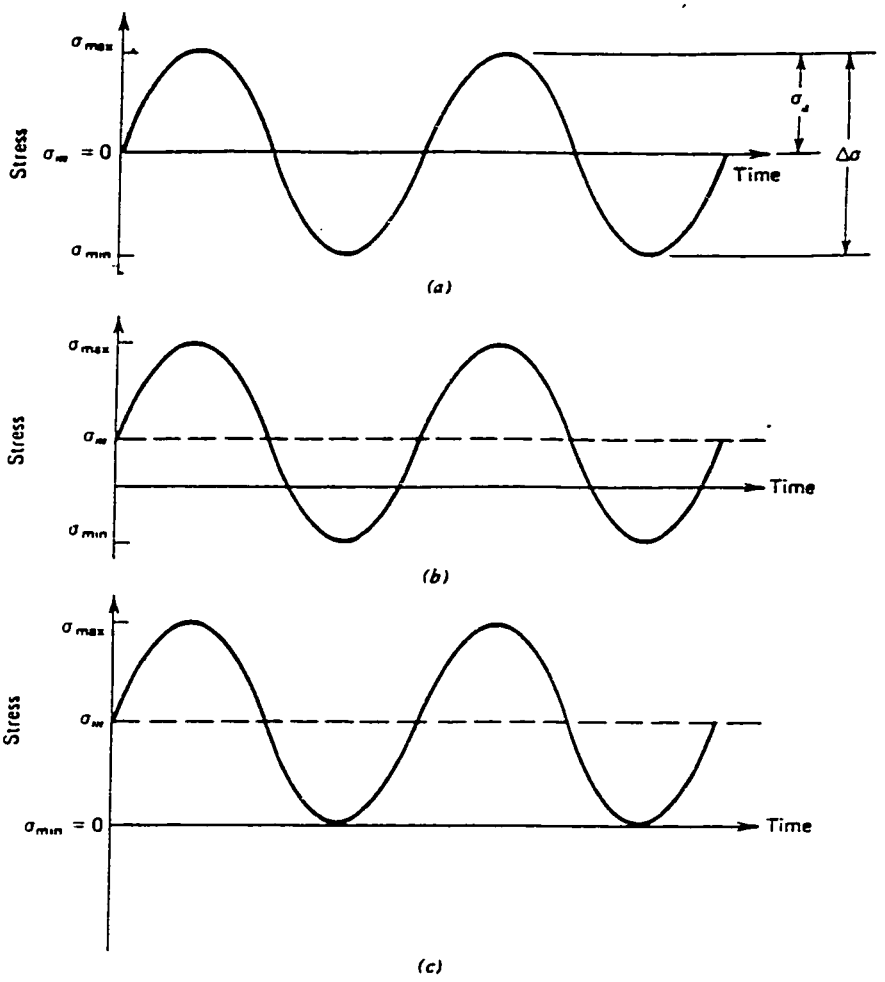

Figure 2.5 Several constant-amplitude stress time patterns of interest. (a) Completely reversed, *SR*= -1. (b) Nonzero mean stress. (c) Zero compression, *SR*= 0 [5].

σ_a is the alternating range of stress ($\frac{\sigma_{max} - \sigma_{min}}{2}$)

$\Delta\sigma$ is the stress range ($\sigma_{max} - \sigma_{min}$)

SR is the stress ratio ($\frac{\sigma_{min}}{\sigma_{max}}$)

A is the amplitude ratio ($\frac{\sigma_a}{\sigma_{min}} = \frac{1 - SR}{1 + SR}$)

Any two of the quantities just defined, except the combination σ_a and $\Delta\sigma$ or the combination A and SR, are sufficient to completely describe the stress-time pattern shown.

A second type of stress-time pattern often encountered is the nonzero mean spectrum shown in Fig. 2.5(b). This pattern is very similar to completely reversed case except that the mean stress is tensile or compressive, in any event different from zero. The nonzero mean case may be thought of as a static stress equal in magnitude to the mean σ_m, with a superposed completely reversed cyclic stress of amplitude σ_a.

A special case of nonzero mean stress, illustrated in Fig. 2.5(c) is often encountered in practice. In this special case the minimum stress σ_{min} is zero. That is, the stress ranges from zero up to some tensile maximum and then back to zero. This type of stressing is often called released tension. For released tension, it may be noted that the mean stress is half the maximum stress, or $\sigma_m = \frac{\sigma_{max}}{2}$. A similar but less frequently encountered stress-time pattern is called released compression, where $\sigma_{max} = 0$ and $\sigma_m = \frac{\sigma_{min}}{2}$.

2.4.3 *S-N-P* Curves — A basic design tool

Basic fatigue data in the high-cycle life range can be conveniently displayed on plot of cyclic stress level versus the logarithm of life, or alternatively, on a log-log plot of stress versus life. These plots, called *S-N* curves, constitute design information of fundamental importance for machine parts subjected to repeated loading. Because of the scatter of fatigue life data at any given stress level, it must be recognized that there is not only one *S-N* curve for a given material, but a family of S-*N* curves with probability of failure as the parameter. These curves are called the *S-N-P* curves, or curves of constant probability of failure on a stress versus life plot.

To develop an *S-N-P* plot in the fatigue laboratory by " standard" methods, one would proceed in the following way:

1. Select a large group of carefully prepared, polished fatigue specimens of the material of interest and, subdivide them into four or five smaller groups of at least 15 specimens each.
2. Select four or five stress levels, perhaps judged by few exploratory tests that span the stress range of the *S-N* curve.
3. Run an entire subgroup at each of the selected stress levels following the procedures to be outlined here.
4. To make each test run, mount a specimen in the testing machine, using due care to avoid spurious stresses. Set the machine for the desired stress amplitude, with cycle counter set to zero.
5. Start the machine and run the constant stress amplitude until the specimen fails or the machine reaches a predetermined *runout* criterion.
6. Record the stress amplitude used and the cycle count at the time of failure or runout.
7. Using a new specimen, repeat the procedure, again recording the stress level and the life at failure or runout. Continue to repeat this procedure until all specimens designated for the selected stress level have been tested.

8. Change to new stress level and repeat the preceding procedure until all specimens designated for the second stress levels have been tested. Repeat this procedure until all selected stress levels have been tested. Note that the entire output from a complete fatigue test is averaged as a single point on the *S-N* plot.
9. Plot all data collected on a stress versus log-life coordinate system as shown in Fig. 2.6. A small arrow to the right indicates runouts, or points for which fatigue failure was not observed during the test.

Considering the data plotted in Fig. 2.6, one could simply construct a visual mean curve through the data. Doing this, it becomes clear that a substantial scatter of data about the mean clouds the design usefulness of such a mean curve. A better approach would be to construct for each stress level a histogram, such as the one shown in Fig. 2.7, which shows the distribution of failures as function of the log life for the sample tested. Computation of the sample mean and variance permits the estimation of population mean and variance if the form of the distribution is known for fatigue tests at a constant stress level. Extensive testing of large samples has indicated that a lognormal distribution of life at a constant stress level is a good estimate. Assuming the life distribution to be lognormal, the sample mean and variance can be used to specify any desired probability of failure. Repeating the analysis at all stress levels, we can connect points of equal probability of failure to obtain curves of constant probability of failure on the *S-N* plot. Such a family of *S-N-P* curves is shown in Fig. 2.8. It is also of interest to note that the "reliability" R is defined to be 1 minus the probability of failure; hence, $R = (1\text{-}P)$. It should be noted that references to the " *S-N* curves" in the literature generally refer to the mean curve unless otherwise specified.

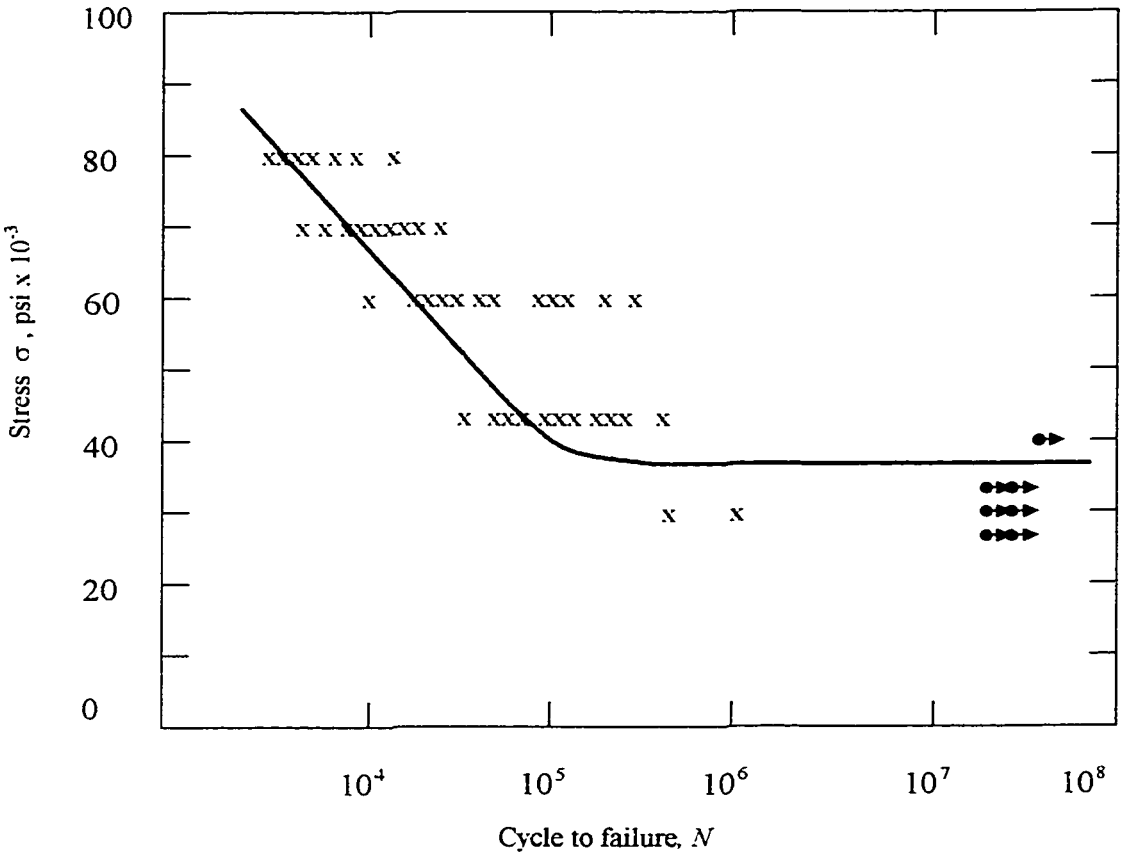

Figure 2.6 Plot of stress-cycle (*S-N*) data as it might be collected by laboratory fatigue testing [5].

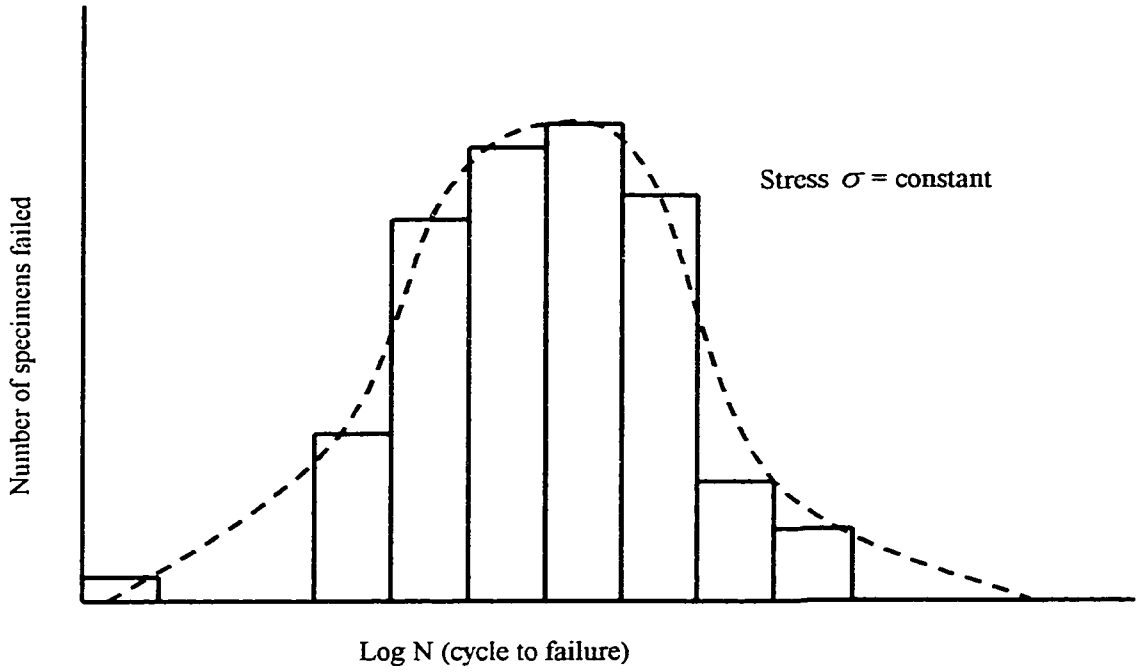

Figure 2.7 Distribution of fatigue specimens failed at a constant stress level as a function of logarithm of life [5].

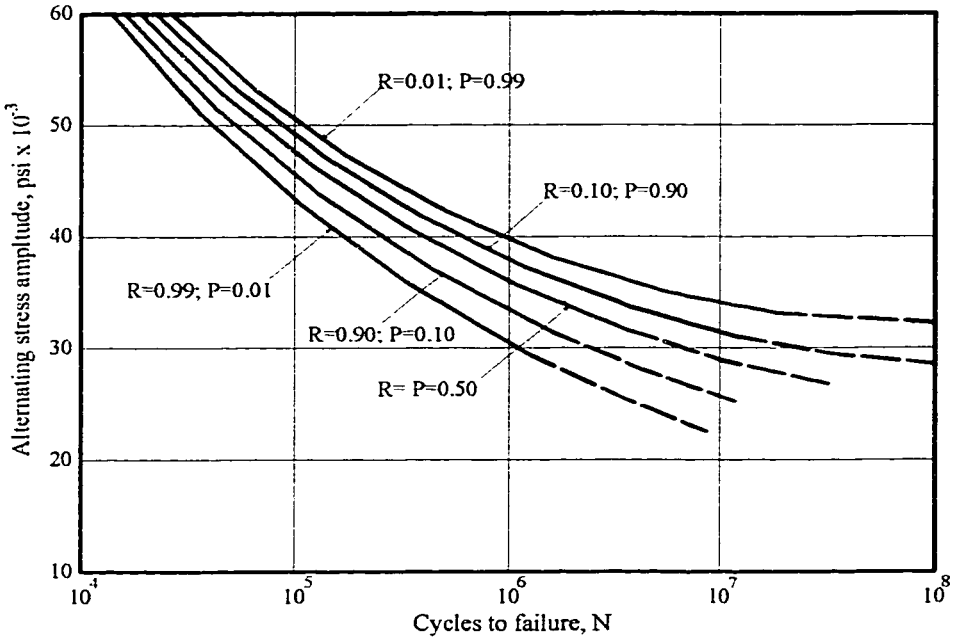

Figure 2.8 Family of *S-N-P* curves. Note P = probability of failure; R= reliability = 1-P. [5].

The mean *S-N* curves sketched in Fig 2.9 distinguish two types of material response to cyclic loading commonly observed. Ferrous alloys and titanium exhibit a steep branch in the relatively short life range, leveling off to approach a stress to asymptote at longer lives. This stress asymptote is called the fatigue limit (formerly called endurance limit) and is the stress level below which an infinite number of cycles can be sustained without failure. The nonferrous alloys do not exhibit an asymptote, and the curve of stress versus life continues to drop off indefinitely. For such alloys, there is no fatigue limit, and failure as result of cyclic load is only a matter of applying enough cycles. All materials, however, exhibit a relatively flat curve in the long life range.

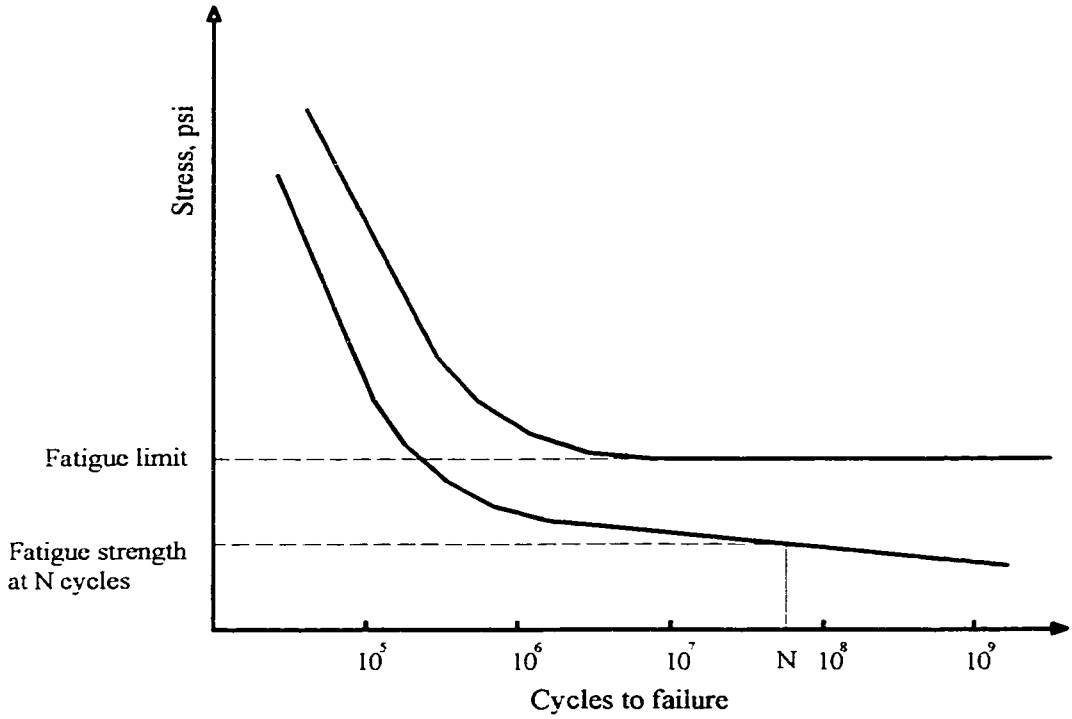

Figure 2.9 Two types of material of cyclic response to cyclic loading [5].

2.5 Strain-life approach

2.5.1 Introduction

The strain-life method is based on the observation that in many components the response of the material at critical locations (notches) is strain or deformation dependent. When load levels are low, stresses and strains are linearly related. Consequently, in the elastic range, load-controlled and strain controlled test results are equivalent. At high levels, in the low-cycle fatigue (LCF) regime, the cyclic stress-strain response and the material behavior are best modeled under strain-controlled conditions [3].

In the strain-life approach, the plastic strain or deformation is directly measured and quantified. As discussed previously, the stress-life approach does not account for plastic strain. At long lives, where plastic strain is negligible and stress is easily related to strain, the strain-life and stress-life approaches are essentially the same.

Although most engineering structures and components are designed such that the nominal loads remain elastic, stress concentrations often cause plastic strains to develop in the vicinity of notches. Due to the constraint imposed by the elastically stressed material surrounding the plastic zone, deformation at the notch root is considered strain-controlled.

The strain-life method assumes that smooth specimens tested under strain-control can simulate fatigue damage at the notch root on an engineering component. Equivalent fatigue damage is assumed to occur in the material at the notch root and in the smooth specimen when both are subjected to identical stress-strain histories. As seen in Fig.2.10, the laboratory specimen models an equally stressed volume of material at the notch root.

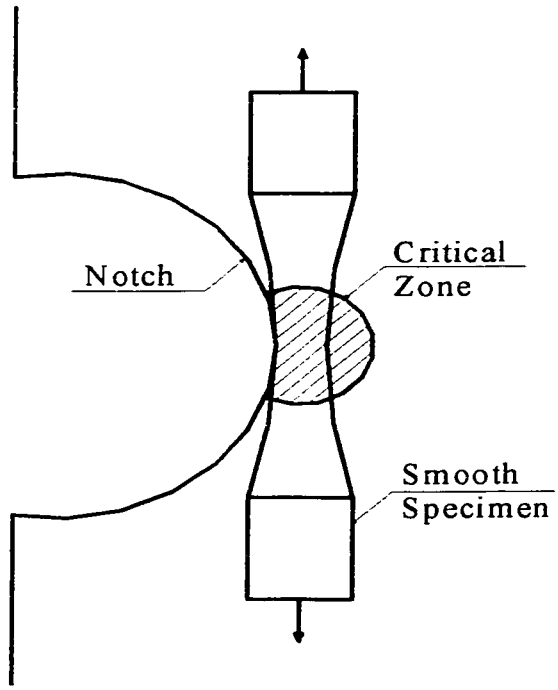

Figure 2.10 Equally stressed volume of material Ref [3].

Crack growth is not explicitly accounted for in the strain-life method. Rather, failure of the component is assumed to occur when the equally stressed volume of material fails. Because of this, strain-life methods are often considered as initiation life estimates. For some applications, the existence of a crack is an overly conservative criterion for component failure. In these situations, fracture mechanics methods may be employed to determine crack propagation life from an assumed initial crack size to a final length. Total lives are reported as the sum of the initiation and propagation segments.

The local strain-life approach has gained acceptance as a useful method of evaluating the fatigue life of a notched component. Both the American Society for Testing Materials (ASTM) and the Society of Automotive Engineers (SAE) have recommended procedures and practices for conducting strain-controlled tests and using these data to predict fatigue lives.

2.5.2 Material behavior

2.5.2.1 Stress-strain relationships

The total true strain ε_t in tension test can be separated into elastic and plastic components:

1. Linear elastic strain: portion of strain, which is recovered upon unloading, ε_e
2. Plastic strain: portion, which cannot be recovered on unloading, ε_p

   (Fig 2.11).

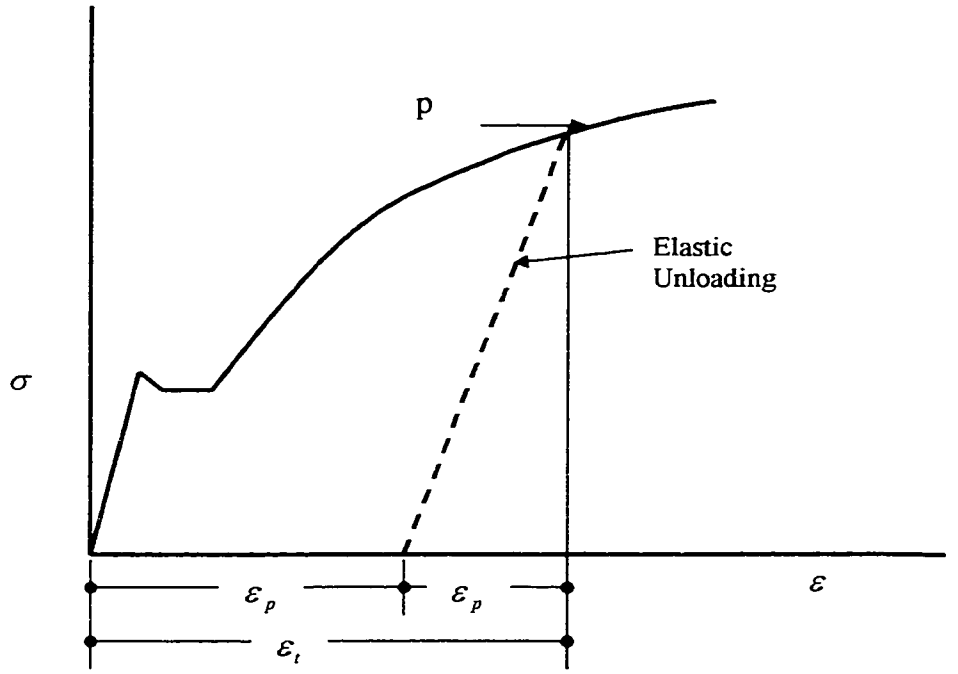

Figure 2.11 Elastic and plastic strain [3]

Stated in equation form,

$$\varepsilon_t = \varepsilon_e + \varepsilon_p \tag{2.8}$$

For most metals a log –log plot of true stress versus true plastic strain is modeled as a straight line; consequently, this curve can be expressed using a power function

$$\sigma = K(\varepsilon_p)^n \tag{2.9}$$

or

$$\varepsilon_p = \left(\frac{\sigma}{K}\right)^{\frac{1}{n}} \tag{2.10}$$

where K is the strength coefficient and n is the strain-hardening exponent.

At fracture two important quantities can be defined (Fig. 2.12). These quantities are the true fracture strength and true fracture ductility. True fracture strength, σ_f, is the true stress at final fracture.

$$\sigma_f = \frac{P_f}{A_f} \tag{2.11}$$

where A_f is the area at fracture and P_f is the load at fracture.

True fracture ductility, ε_f, is the true strain at final fracture. This value can be defined in terms of the initial cross-sectional area and the area at fracture.

$$\varepsilon_f = \ln\frac{A_0}{A_f} = \ln\frac{1}{1-RA} \tag{2.12}$$

$$RA = \frac{A_0 - A_f}{A_0} = \text{reduction in area} \tag{2.13}$$

The strength coefficient, K, can be defined in terms of the true stress at fracture, σ_f, and the true strain at fracture, ε_f.

Substituting σ_f and ε_f into Eq. 2.9 yields

$$\sigma_f = K(\varepsilon_f)^n \tag{2.14}$$

Rearranging

$$K = \frac{\sigma_f}{\varepsilon_f^n} \tag{2.15}$$

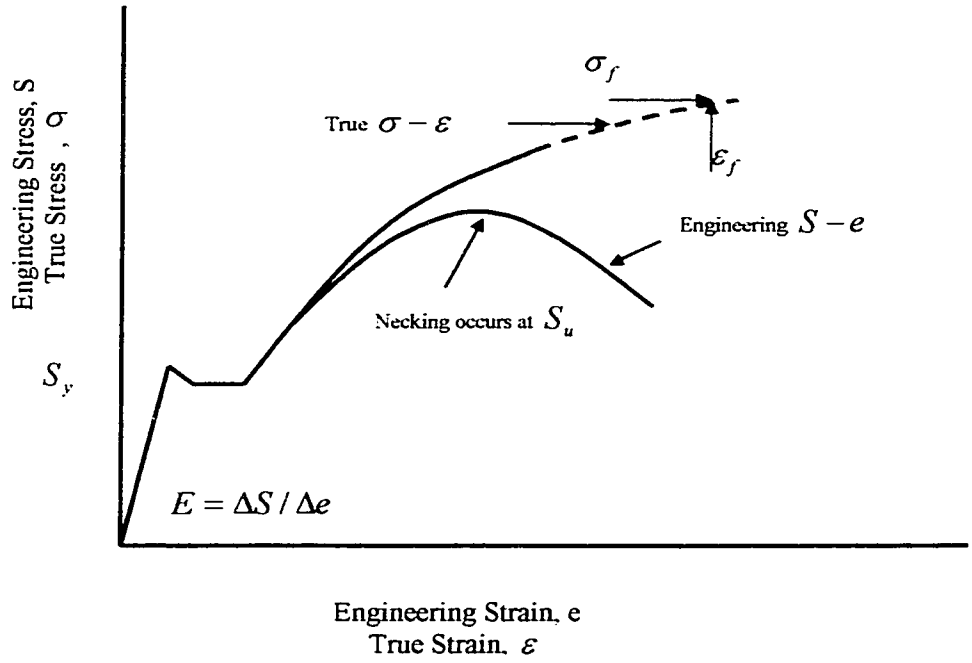

Figure 2.12 True stress versus true strain and engineering stress versus engineering strain [3].

We can also define plastic strain in terms of these quantities. Combining Eqs. 2.15 and 2.10, we have

$$\varepsilon_p = \left(\frac{\sigma}{\frac{\sigma_f}{\varepsilon_f^n}} \right)^{\frac{1}{n}} \tag{2.16}$$

therefore

$$\varepsilon_p = \varepsilon_f \left(\frac{\sigma}{\sigma_f} \right)^{\frac{1}{n}} \tag{2.17}$$

The elastic strain is defined as

$$\varepsilon_e = \frac{\sigma}{E} \tag{2.18}$$

Therefore we may state that:

$$\varepsilon_t = \frac{\sigma}{E} + \left(\frac{\sigma}{K} \right)^{\frac{1}{n}} \tag{2.19}$$

where:

E is the modulus of elasticity.

2.5.2.2 Cyclic stress-strain behavior

Monotonic stress-strain curves have long been used to obtain design parameters for limiting stresses on engineering structures and components subjected to static loading. Similarly, cyclic stress-strain curves are useful for assessing the durability of structures and components subjected to repeated loading [3].

The response of material subjected to cyclic inelastic loading is in the form of a hystersis loop, Fig. 2.13. The total width of the loop is $\Delta\varepsilon$ or the total strain range. The total height of the loop is $\Delta\sigma$ or the total stress range.

These can be stated in terms of amplitude:

$$\varepsilon_a = \frac{\Delta\varepsilon}{2} \tag{2.20}$$

where:

ε_a is the strain amplitude and

$$\sigma_a = \frac{\Delta\sigma}{2} \tag{2.21}$$

where:

σ_a is the stress amplitude.

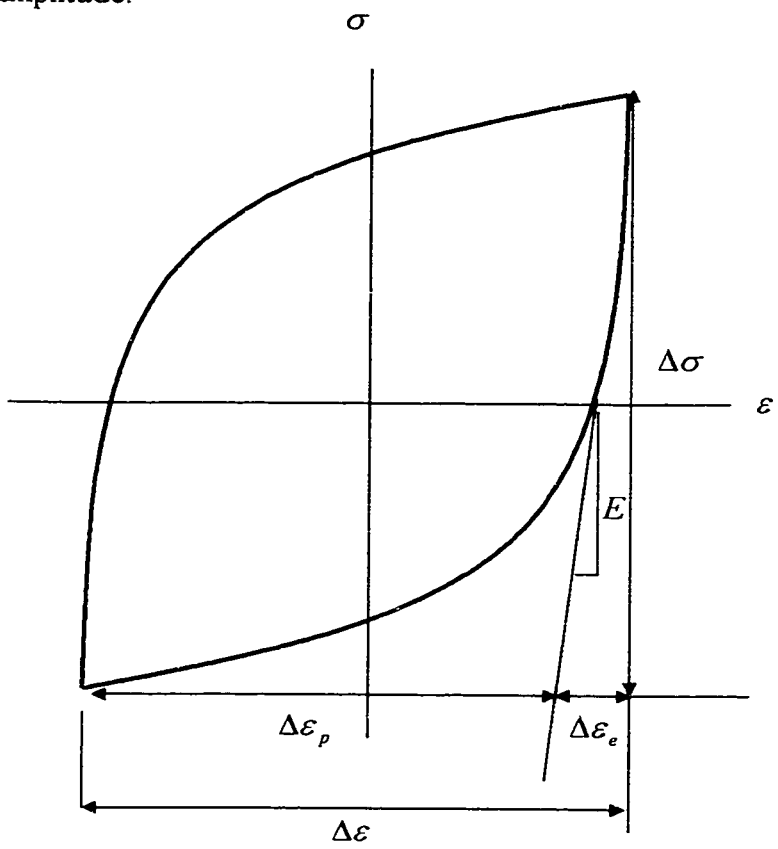

Figure 2.13 Hysteresis loop Ref [3].

The total strain is the sum of the elastic and plastic strain ranges,

$$\Delta\varepsilon = \Delta\varepsilon_e + \Delta\varepsilon_p \tag{2.22}$$

or in terms of amplitude,

$$\frac{\Delta\varepsilon}{2} = \frac{\Delta\varepsilon_e}{2} + \frac{\Delta\varepsilon_p}{2} \tag{2.23}$$

Using Hooke's law, the elastic term may be replaced by $\Delta\sigma/E$.

$$\frac{\Delta\sigma}{2} = \frac{\Delta\sigma}{2E} + \frac{\Delta\varepsilon_p}{2} \tag{2.24}$$

The area within the loop is the energy per unit volume dissipated during a cycle. It represents a measure of the plastic deformation work done on the material.

2.5.2.3 Stress-plastic strain power law relation

A log-log plot of the completely reverse3d stabilized cyclic true stress versus true plastic strain can be approximated by a straight line (Fig. 2.14):

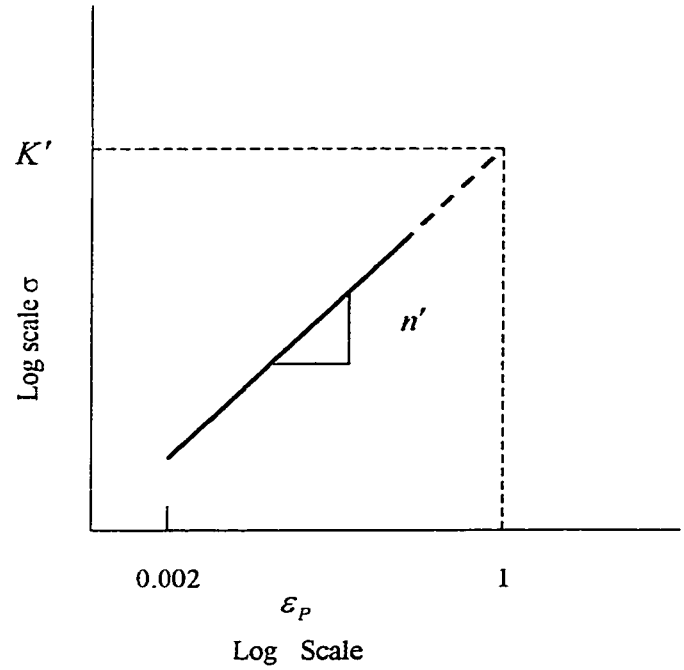

Figure 2.14 Log-log plot of true cyclic stress versus true cyclic plastic strain [3].

We can develop a power law function,

$$\sigma = K'(\varepsilon_p)^{n'} \tag{2.25}$$

where σ is the cyclically stable stress amplitude

ε_p is the cyclically stable plastic strain amplitude

K' is the cyclic strength coefficient

n' is the cyclic strain-hardening exponent

For most metals the value of n' usually varies between 0.10 and 0.25, with an average value close to 0.15. Rearranging Eq. 2.25 gives

$$\varepsilon_p = \left(\frac{\sigma}{K'}\right)^{1/n'} \tag{2.26}$$

The total strain is the sum of the elastic and plastic components. Using Eq. 2.42 and Hooke's law, the total strain can be written

$$\varepsilon = \frac{\sigma}{E} + \left(\frac{\sigma}{K'}\right)^{1/n'} \tag{2.27}$$

It is to be noted that the relationship between the strain amplitude and the number of cycles is presented in section 2.3.

2.6 Fracture mechanics approach

2.6.1 Introduction

Fatigue design for many components is a process of design to prevent the initiation of crack. For many components this represents the total design life, either because a crack will propagate so rapidly that life to crack initiation represents almost the total life, or because product liability legislation precludes the release into service of components, which develop cracks during service even though the component may still achieve its design life.

This design philosophy cannot be applied to all components. For example, aircraft structures can experience accidental damage in flight, and crack growth calculations must demonstrate that the structure is airworthy after impact damage. Other components may develop cracks in service as a result of design errors, and it may then be necessary to calculate safe inspection intervals to prevent the cracks causing catastrophic fracture [6].

The study of predominantly brittle fracture from short cracks and defects is the subject of *Fracture Mechanics*.

2.6.2 Purpose of fracture mechanics

A structure may develop a fatigue crack under repeated service loading. As the crack length increases, it causes a greater stress concentration, and so the rate of crack propagation increases. The strength of the structure is reduced as the crack length increases. Eventually, the strength of the structure will be insufficient to withstand the highest service loads, and failure is possible if the highest service load occurs. As the crack continues to grow, the structural strength will be reduced until the structure cannot withstand the normal service loads, and so fracture under normal loading becomes very probable.

Faced with design problem the designer must be able to calculate the following criterion to check against crack (Fig. 2.15):

1. The residual strength as a function of crack size
2. The crack size that can be allowed at the expected service load (the critical size)
3. How long it takes the crack to grow from a certain size to a critical size
4. The size if initial flaws that can be tolerated in a new component
5. The interval between inspections for cracks

Fracture mechanics tries to provide tools with which to answer these questions. The subject includes the materials science studies of fracture processes on an atomic scale, the growth of cracks, the analysis of the crack tip tresses and the behavior of cracks in these stress fields, the provision of materials properties by testing, and finally the engineering application of these techniques to the analysis of real structures.

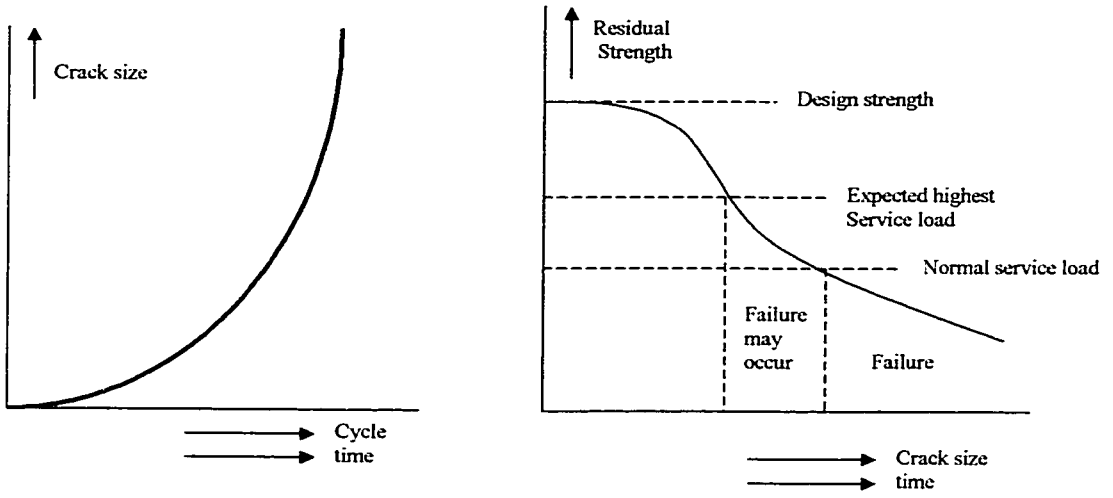

Figure 2.15 Relationship between crack length and failure load [6].

2.6.3 Stresses at the crack tip

A crack can be stressed in three different modes, Mode I is the normal or opening mode, Mode II is the tearing mode caused by in-plane shear, and Mode III is the tearing mode caused by out-of-plane shear (Fig. 2.16).

Most problems can be addressed by superimposing one or more of these modes, but Mode I is by far the most important for practical analysis.

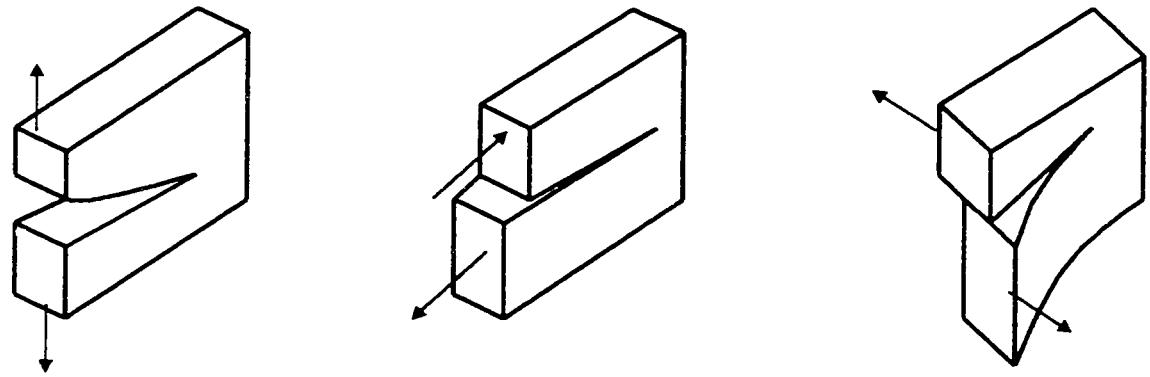

Figure 2.16 The three crack opening modes [6].

For arbitrary through-thickness crack of size a, in a body of arbitrary shape and loaded by arbitrary Mode I loading, the stress distribution near the crack tip is represented in Fig. 2.17.

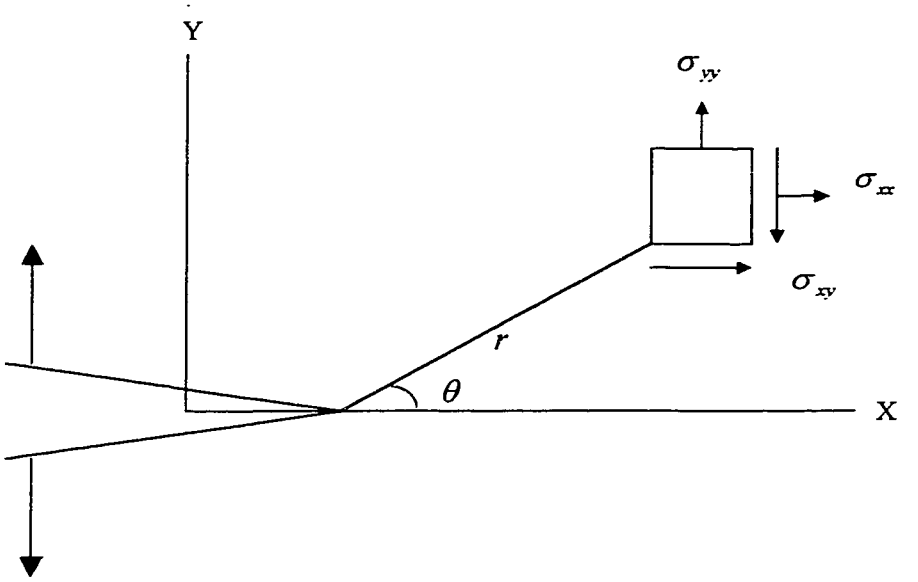

Figure. 2.17 Generalized stresses at the crack tip [6].

It would be expected that stresses reduce with increasing r, and will be a function of the angle θ. The general expression for the stress field is

$$\sigma_{ij} = \frac{K_I}{\sqrt{2\pi r}} fij(\theta) \tag{2.28}$$

where σ_{ij} are the stresses acting on an element $dxdy$ at a distance r from the crack tip at an angle θ from the crack plane, and $f_{ij}(\theta)$ are known functions of θ. The factor K_I is as yet unknown, because the loading and the shape of the body are yet to be defined.

As it appears that the entire stress field close to the crack tip can be described if K_I is known, K_I is an important parameter called the stress intensity factor and the subscript I denotes mode I loading.

Eq. 2.28 can be applied to an infinite plate subjected to uniform tension, with a central crack of length $2a$.

The standard convention is to let the length of the crack equal to $2a$ if the crack has two tips, and equal to a if the crack has one tip Fig. 2.18. As the left hand side of Eq. 2.28 has unit of stress, and as $f(\theta)$ has no units, then $\frac{K_I}{\sqrt{2\pi r}}$ must have units of stress, and so K_I must have a unit of stress multiplied by square root of length. As the only stress is the remote stress, and as the only length is the crack length a, then

$$K_I = \beta\sigma\sqrt{a} \tag{2.29}$$

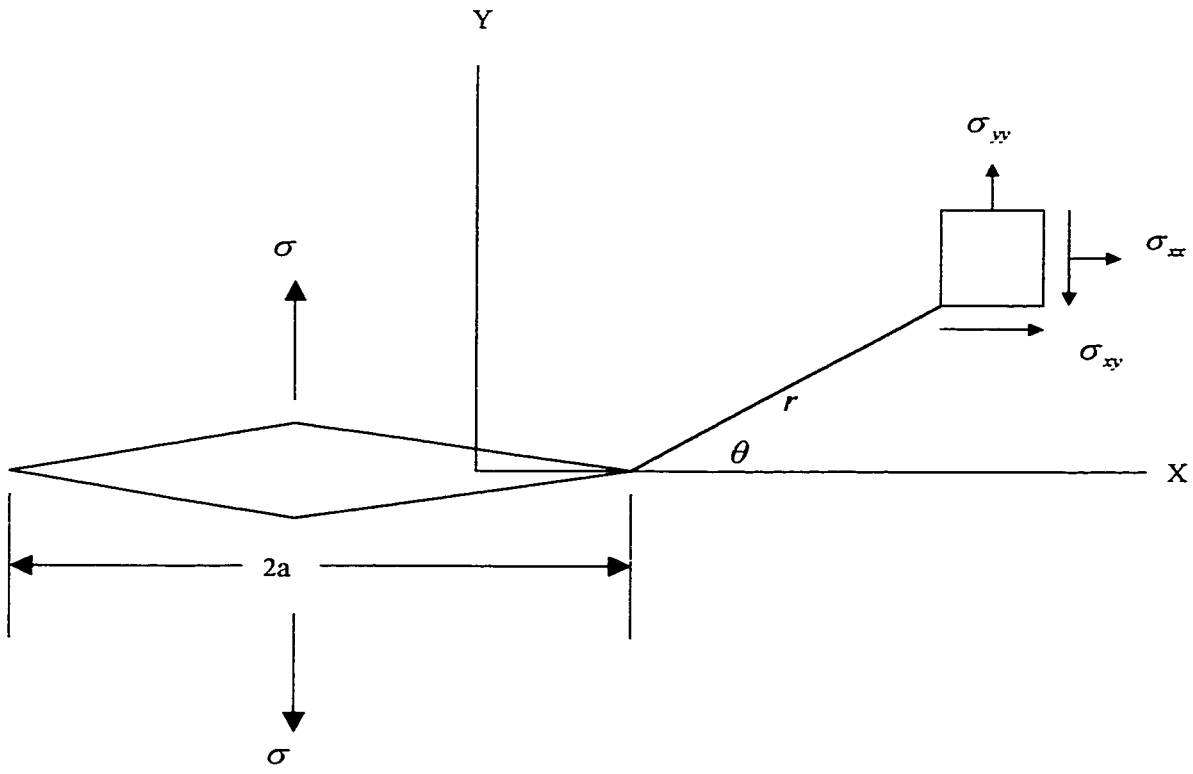

Figure 2.18 Generalized stresses for a crack in an infinite plate [6].

In fact if $\beta = \sqrt{\pi}$ for a center in an infinite plate, but it is convention to refer all stress intensity factors to the infinite plate case, (*i.e* make the constant equal to *1* for this case). Therefore K_I is given by

$$K_I = \beta\sigma\sqrt{\pi a} \tag{2.30}$$

The factor β is a function of the crack dimension a and the shape of the component. Values of β have been giving in [7].

The stress σ in these equations is always the remote stress, not the stress in the cracked section. The fact that the average stress in the net section will be higher is accounted for in the tabulated values of β.

Combining Eqs. 2.28 and 2.30

$$\sigma_{ij} = \beta\sigma\sqrt{\frac{a}{2r}} f_{ij}(\theta) \tag{2.31}$$

For mode *I* loading, the function $f_{ij}(\theta)$ can be added to give

$$\sigma_x = \beta\sigma\sqrt{\frac{a}{2r}}\cos\frac{\theta}{2}\left(1-\sin\frac{\theta}{2}\sin\frac{3\theta}{2}\right)$$

$$\sigma_y = \beta\sigma\sqrt{\frac{a}{2r}}\cos\frac{\theta}{2}\left(1+\sin\frac{\theta}{2}\sin\frac{3\theta}{2}\right) \tag{2.32}$$

$$\sigma_z = \beta\sigma\sqrt{\frac{a}{2r}}\sin\frac{\theta}{2}\cos\frac{\theta}{2}\cos\frac{3\theta}{2}$$

This single set of functions $f(\theta)$ applies to all mode *I* cases. Moreover, Eq. 2.31 provides the stresses close to the crack tip only. It is in fact a truncation of a series

$$\sigma_{ij} = \beta\sigma\sqrt{\frac{a}{2r}} + 2^{nd}\text{ term} + 3^{rd}\text{ term} + \ldots\ldots \tag{2.33}$$

For small values of r, the first term tends to infinity but the remaining terms tend to zero, and so can be neglected. Using only the first term implies that the stresses tend to zero at

large values of r . In fact they tend to σ, the remote stress. Hence the need for the 2nd and subsequent terms at large values of r.

2.6.4 Fracture toughness

Eq. (2.28) $\sigma_{ij} = \frac{K_I}{\sqrt{2\pi r}} fij(\theta)$, applies to all different cracked bodies. If the load is increased until fracture occurs, then the fracture stress from the mentioned equation can be substituted into the equation $K_I = \beta\sigma\sqrt{\pi a}$. The value of K_I at fracture is called the fracture toughness.

Fracture occurs when the value of K_I equals the fracture toughness value. It is therefore a similitude parameter. Fracture occurs at a particular value of K_I whatever the shape of the body or size of the crack.

2.6.5 Plasticity

Eq. 2.28 is an elastic equation and implies that the crack tip stresses become infinite at the crack tip, that is $r = 0$. This cannot be true, and in fact plastic deformation occurs which keeps the crack tip stress finite.

A first estimate of the size of the plastic zone can be obtained from diagram such as Fig.2.19 by determining the distance from the crack tip (r_p^*) over which the stresses exceed the yield stress for the material.

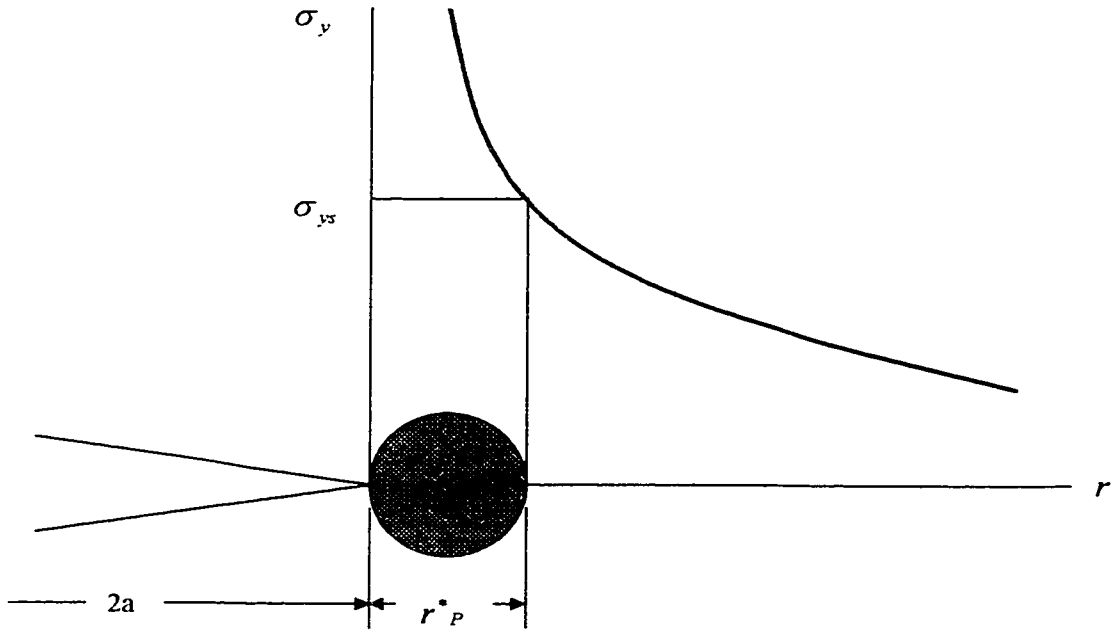

Figure 2.19 Plastic zone at the crack tip [6].

Substituting $\sigma_y = \sigma_{ys}$ into Eq. 2.28 gives:

$$\sigma_y = \frac{K_I}{\sqrt{2\pi r_p^*}}$$

so that

$$r_p^* = \frac{K_I^2}{\sqrt{2\pi\sigma_{ys}^2}}$$

In fact the size of the plastic zone is lager (Fig 2.20).

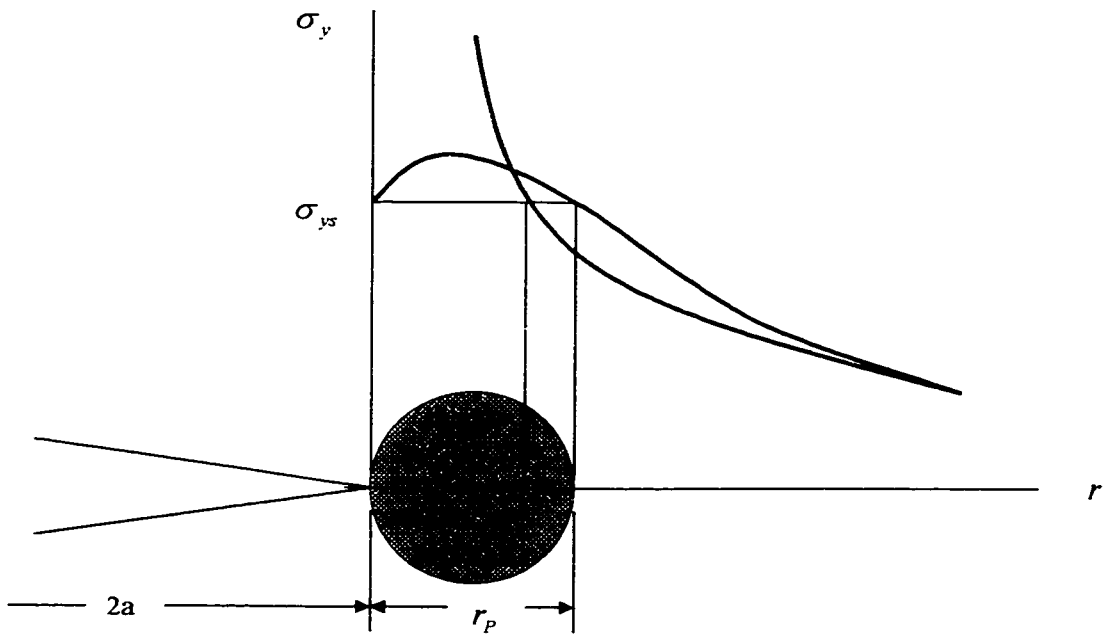

Figure 2.20 More accurate estimate of crack tip plastic zone size [6].

However, the approximate value, r_p^*, has the advantage that it can be obtained directly from the stress intensity factor and the yield stress. K_I still represents a similitude parameter, provided the size of the plastic zone is still determined by K_I. In other words, plasticity must be restricted to an area close to the crack tip that is the area where the 2nd and subsequent terms in Eq. 2.33 can be neglected.

2.6.6 Crack propagation

The preceding sections have concentrated on the calculation of final fracture. However, it is possible that the applied stress on a crack may cause the crack to extend a small amount, without causing fracture.

If the applied load varies between zero and some value (constant amplitude cycling) the stress intensity K varies over a range ΔK. The rate of crack propagation da/dN must depend on the range of the stress intensity ΔK so that

$$\frac{da}{dN} = f(\Delta K) = f(2S_a\sqrt{\pi a}) \tag{2.34}$$

where S_a is the stress amplitude (Fig. 2.21) and N is the number of cycles.

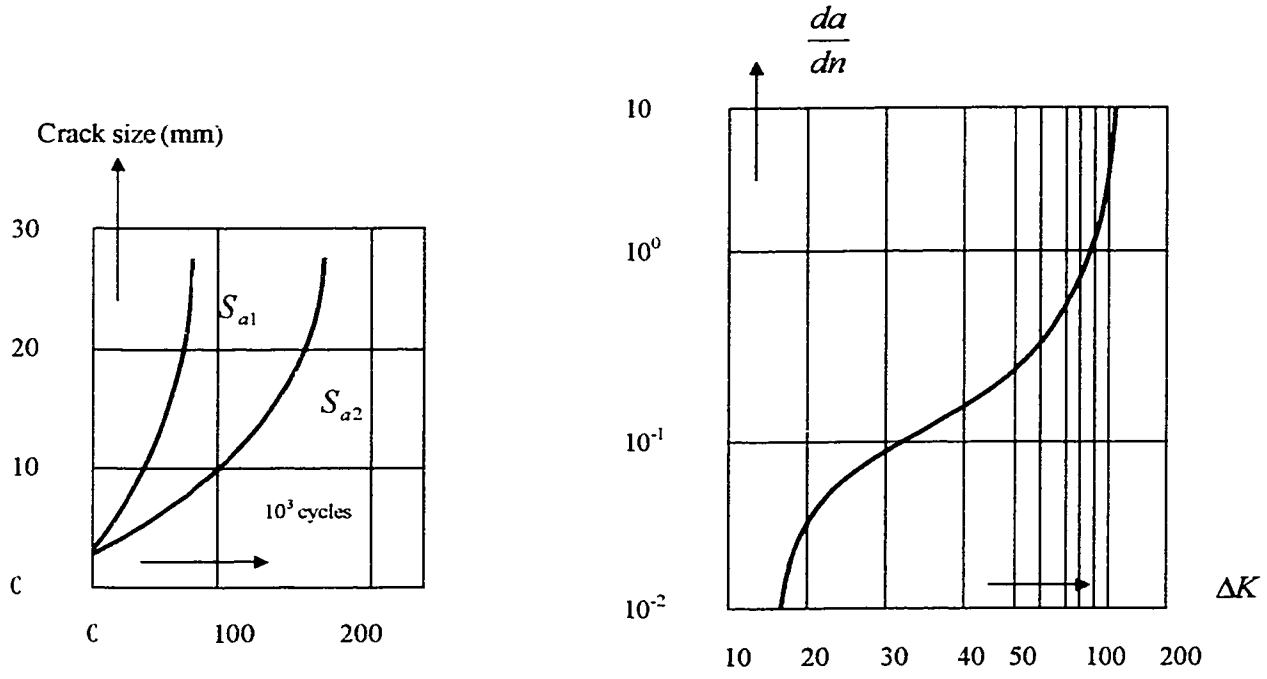

Figure 2.21 Crack propagation diagrams [6].

The results of the tests (Fig 2.21(*a*)), for two different stress amplitudes, can be plotted on the basis of *da/dN* at the instantaneous value of ΔK. In (*b*) the data has been plotted on a log-log basis.

The fact that both sets of data fall on the same curve shows that Eq. 2.34 applies for small cracks at the high stress, or large cracks at low stress. The two cracks have the same growth rate providing the values of ΔK together with two material constants. The central part of the curve in (*b*) is the approximately straight line and for this central region, Eq. 2.34 can be re-written as

$$\frac{da}{dN} = C(\Delta K)^n \tag{2.35}$$

Equation 2.30, $K_I = \beta\sigma\sqrt{\pi a}$, allows values of ΔK to be calculated for any combination of crack geometry and remote stress, and these two equations are the fundamental crack growth equations.

Chapter 3

Criteria for Fatigue Life Predictions

3.1 Overview of multiaxial fatigue theories

Although the three-dimensional local stress-strain field response can be determined by finite element method, the proper approach to strain based multiaxial fatigue analysis is not clear. Several multiaxial fatigue theories have been suggested in the literature, two of which had been explained in Chapter 2. However, there exists a lack of agreement on which model is most appropriate.

There are five fatigue theories which engineers can rely on to calculate the fatigue resistance of structural components. Three commonly used approaches, the maximum principal strain, the maximum shear strain and the effective strain, are based on extensions of static yield criteria and two theories, the critical plane approaches, are based on critical damage planes. A common characteristic of all five approaches is that the required material properties can be determined from standard uniaxial fatigue test data. Also, the fatigue life prediction of multiaxially loaded component is based on the uniaxial relationship between the strain amplitude and the number of cycles, namely the Manson-Coffin equation.

In an effort to evaluate the validity of these theories, Fash [7] performed analytical and experimental analyses in which he used finite element method to evaluate the three dimensional stress-strain fields. The obtained strains were used to predict the fatigue life of the Society of Automotive Engineerings (SAE) (Fig. 3.1) notched shaft using all five theories. Comparing the experimental cycles to the predicted cycles, Fash found that the correlation of all five methods is within a factor of ten. He argued that the lack of perfect correlation is related to the effect of the notch on the local stress-strain field and actual damage mechanisms.

In a later study Fash's work was investigated by Hoffman and Seeger [12]. In their study, they have used finite element method as well as Neuber's rule to calculate the local stress-strain fields. They only investigated the maximum principal strain; equivalent strain and the maximum shear strain. It was concluded that the predicted cycles agree with the experimental results within a range of factor of three and the maximum strain parameter delivers the best correlation. They argued that the larger scatter of Fash's results was caused by the finite element mesh where he only used one element at the notch due to the lack of computer resources. To further investigate the issue, the SAE notched shaft has been reanalyzed in this thesis. Fig.3.2.

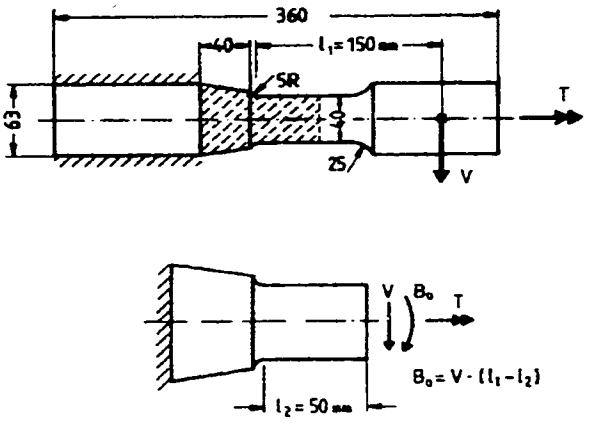

Figure 3.1 SAE notch shaft geometry and loading.
Ref [12]

3.2 Shaft analysis by finite element method

3.2.1 Analysis overview

In an effort to evaluate the predictive capabilities of several multiaxial fatigue theories, a series of, bending, torsion and combined bending-torsion tests were conducted by the Society of Automotive Engineerings using the notched shaft Fig. 3.1 [12]. Finite element analyses of the shaft have been conducted here for different loading conditions.

The primary objective is to calculate the local stresses and strains of the same SAE notched shaft using Finite Element Technique. The elastic-plastic finite element analysis is carried out using ABAQUS [9] with nonlinear material behavior. The cyclic stress-strain curve Fig. 3.2, obtained from Eq. 3.1 is represented truly without any linear approximation. Table (3.1) represents the material properties for SAE 1045 steel as reported in the literature [12].

$$\varepsilon = \frac{\sigma}{E} + \left(\frac{\sigma}{K'}\right)^{\frac{1}{n'}} \tag{3.1}$$

Where ε is the total strain

σ is the stress

$K' = \dfrac{\sigma_{f'}}{\varepsilon_{f'}^{n'}}$ is the cyclic strength coefficient

$n' = \dfrac{b}{c}$ is the cyclic hardening exponent

E is the modulus of elasticity

Table 3.1 Smooth Specimen Uniaxial Fatigue Constants of the SAE –1045 steel

Laboratory	*Specimen diameter (mm)*	$\sigma_{f'}$ *(MPa)*	*b*	$\varepsilon_{f'}$	*c*	*E (MPa)*
Ford Motor Company	5.0	1049.0	-0.105	0.229	-0.454	202000

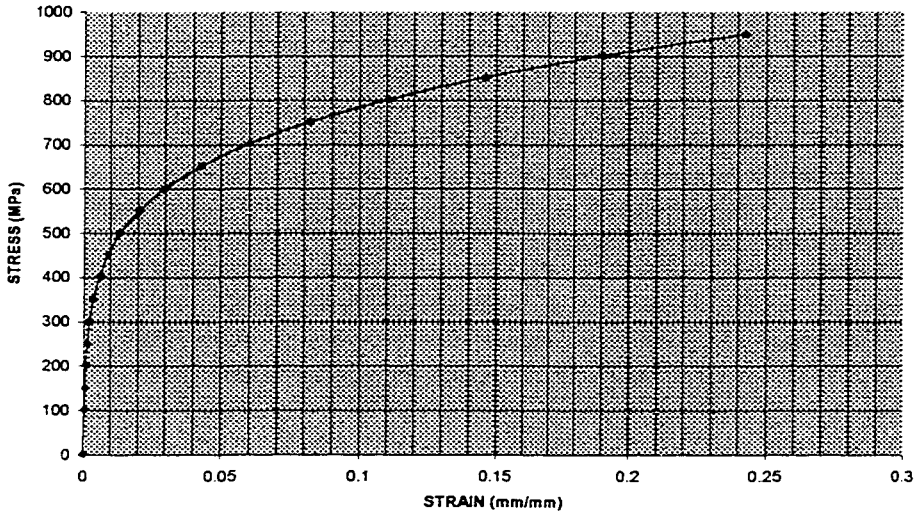

Figure 3.2 Cyclic stress-strain curve.

Figure 3.3 Three-dimensional finite element mesh.

3.2.2 Detail on finite element analysis

The main features of the finite element technique employed are listed below.

1. Isoparametric elements with 20 nodes (quadratic displacement functions)

An overview of solid elements is presented, so that one has a brief but effective explanation of the behavior of various solid elements. ABAQUS [9] contains a library of solid elements for two-dimensional and three-dimensional applications. The two-dimensional elements allow modeling of plane and axisymmetric problems, and include extensions to generalized plane strain (when the model exists between two planes that may move with respect to each other, providing thickness direction strain that may vary with position in the plane of the model but is constant with respect to thickness position).

The solid element library includes isoparametric elements: quadrilaterals in two dimensions and bricks (hexahedral) in three dimensions (Fig. 3.4). These isoparametric elements are generally preferred for most cases because they are usually the more cost-effective of the elements that are provided in ABAQUS. They are offered with first and second order interpolation. For practical reasons, it is sometimes not possible to use isoparamatric elements throughout the model; for example, some commercial mesh generators use automatic meshing techniques that rely on triangulation to fill arbitrarily shaped regions. Because of these needs ABAQUS includes triangular, tetrahedron, and wedge elements.

In this analysis, tetrahedral and hexahedral three-dimensional elements are used. The tetrahedral elements exist due to fact that two-dimensional mesh was rotated 360^0 to obtain three-dimensional solid elements. Moreover, the three-dimensional solid elements are used with second order (quadratic) interpolation. The second order elements are used due to fact that they are capable of representing all possible linear strain fields.
Reduced Gaussian integration (2x2x2 integration points) is also used in this analysis. Reduced integration element C3D20R with lower order integration tends to reduce the

running time compared to the C3D20 element, which has 27 integration points whereas C3D20R element has 8 integration points. Moreover, a reduced integration (low-order) element tends to soften the element thus countering the overly stiff behavior associated with an assumed displacement field.

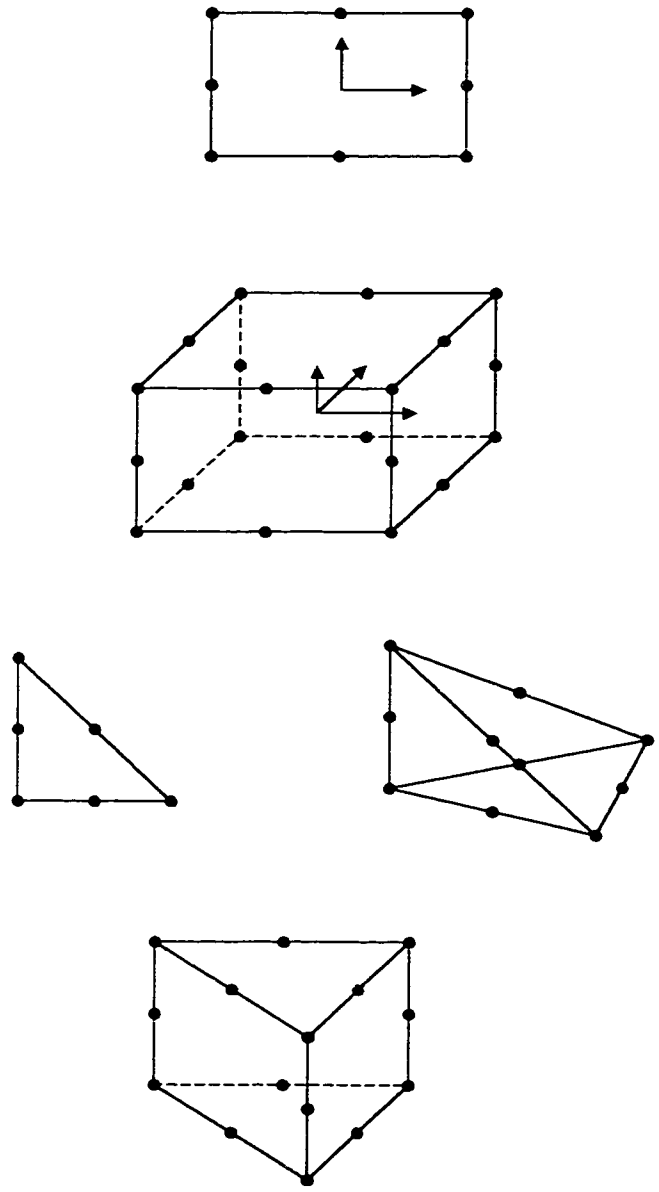

Figure 3.4 Isoparametric master elements

Ref [9]

1. Isotropic hardening with von Mises flow criterion

Isotropic hardening is generally considered to be suitable model for problems in which the plastic straining goes well beyond the incipient yield state where Bauschinger effect is noticeable Fig 3.5. Therefore, the hardening theory is used for such applications. The Mises yield function with associated flow means that there is no volumetric plastic strain; since the elastic bulk modulus is quite large; the volume change will be small [9].

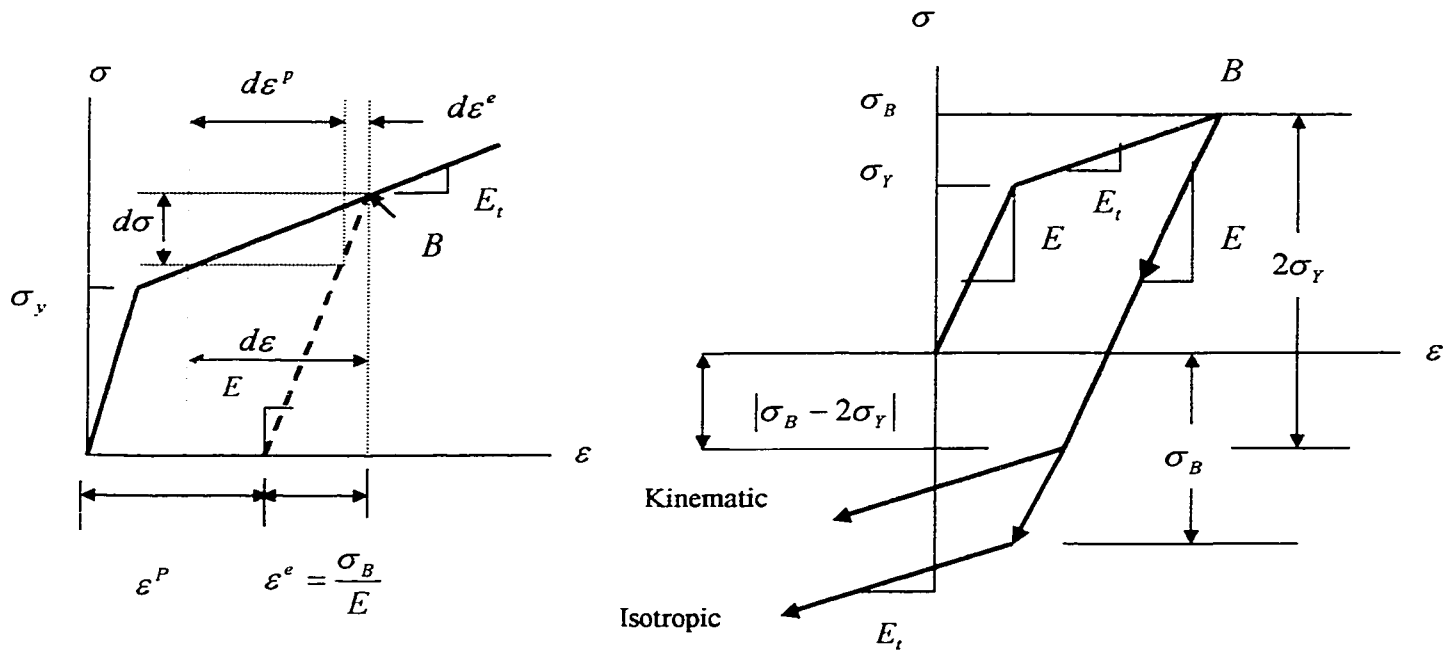

Figure 3.5 (a) Stress-strain plot in uniaxial stress, idealized as two straight lines, (b) Kinematic and isotropic hardening rules. Ref [4].

1. BFGS method for equilibrium iteration

The most frequently used iteration schemes for the solution of nonlinear finite element equations are the Newton-Raphson iteration techniques. However, as an alternative of Newton-Raphson iteration, a class of methods known as matrix update methods or quasi-Newton methods has been developed for iteration on nonlinear systems of equations [1]. These quasi-Newton methods provide a compromise between the full re-formation of the stiffness matrix performed in the full Newton–Raphson method and the use of a stiffness from previous configuration as is done in the modified Newton-Raphson method. Among the quasi-Newton methods available, the BFGS (Broyden-Fletcher-Goldfrab-Shanno) method appears to be most effective regarding computer time and storage.

4. Maximum load

The maximum load is gradually applied by 100 load increments. The constant amplitude load is applied over one unit time Fig. 3.6. The load increments are achieved through ABAQUS input file. ABAQUS automatically adjusts the size of the load so that it solves nonlinear problems efficiently. The •static option is composed of initial time increment ΔT and total step time T. These data in the static option specify the proportion of load applied in the first increment. Therefore, the initial load increment is given by:

$$\left(\frac{\Delta T}{T}\right) * Load\ magnitude$$

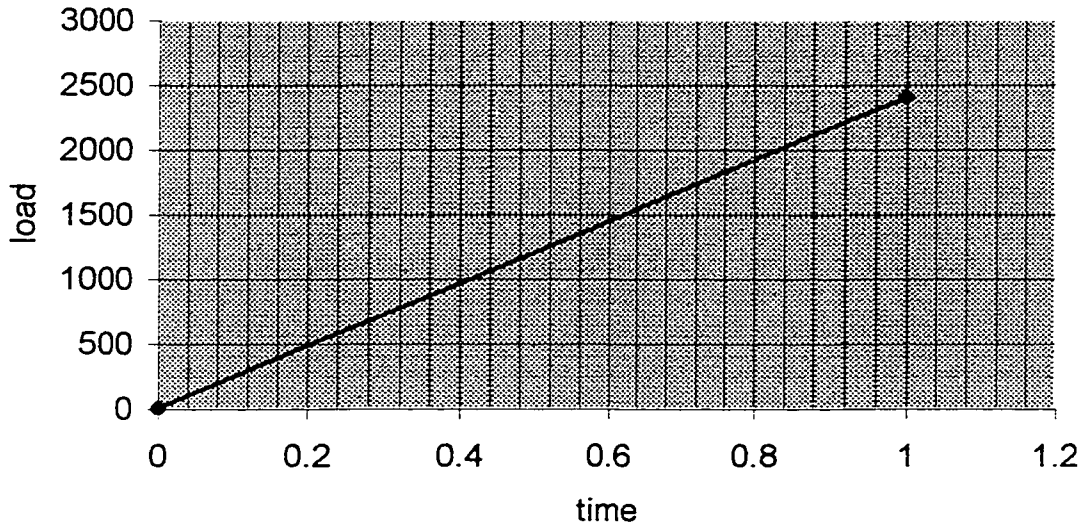

Figure 3.6 Arbitrary constant amplitude load over one unit time

5. Nodal stresses and strains

It is possible to obtain the stresses and strains at the nodes by requesting them from the output request section in ABAQUS input file. These nodal stresses and strains are averaged from all elements that share the same node. The averaged nodal stresses and strains are obtained by interpolation from the integration points. It is worthwhile to notice that it is of necessary to obtain stresses and strains at the nodes since some of these nodes lie on the surface of the components where plastic strains takes place and starts to cause crack initiation Fig. 3.7.

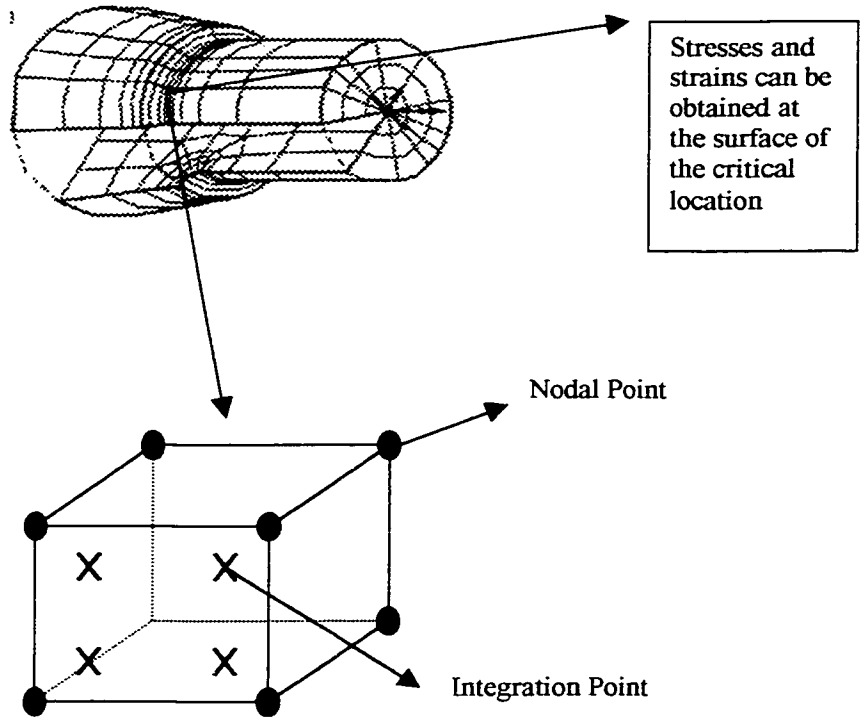

Figure 3.7 A Schematic representation of three-dimensional model

6. Mesh quality and result checks

One of the most important issues in any finite element analysis is meshing quality. Meshing quality is easily checked through the process of meshing generation. In other words, the quality of the mesh is checked through the postprocessor software such as Hypermesh. The elements warpage, aspects ratio, and jacobians can be checked for recommended limits that are provided by the software.

To ensure that the obtained results are reliable, the mesh density of shaft was changed. Purposely, the mesh density at the critical location (notch) was refined from three elements to eight elements Figs 3.8 (model I), and 3.9 (model II). Elastic analyses of the two different mesh densities were performed using the same load. The obtained results did not show a large scatter of the examined parameters, namely, the maximum principal stresses and strains (Table 3.2).

Table 3.2 Comparisons Between Two Different Mesh Densities (Models I and II)

Model	Max Principal Stress	Max Principal Strain	Predicted Cycles
I	767.3 (MPa)	3.566E-03	20098
II	767.0 (MPa)	3.577E-03	19884

Figure 3.8 three-dimensional meshes with three elements at the notch (model I).

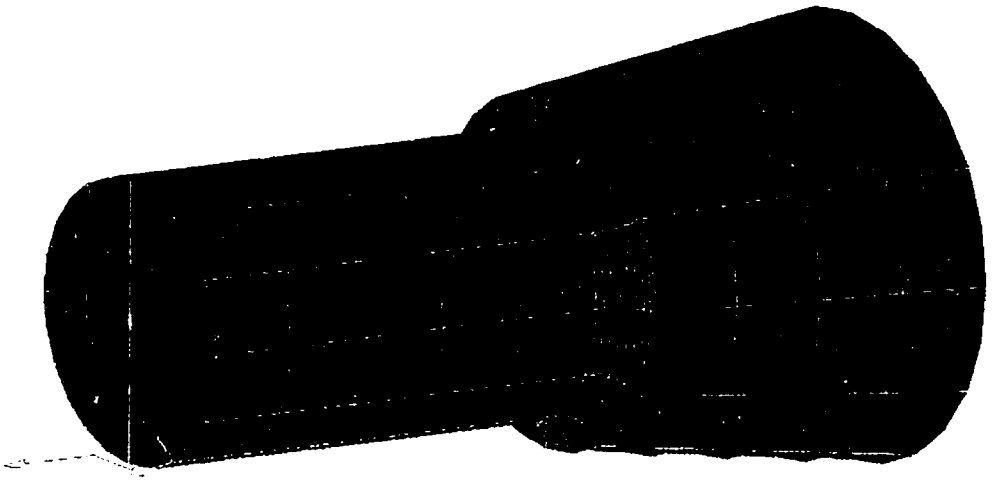

Figure 3.9 Three-dimensional meshes with eight elements at the notch (model II)

3.3 Life Predictions of notched shaft under multiaxial loading

3.3.1 Introduction

The validities of the maximum principal strain and the maximum shear strain criteria are investigated by predicting the fatigue lives of the SAE notch shaft under different multiaxial loadings. The predicted fatigue lives are compared to experimental fatigue lives that are reported in the literature [12].

3.3.2 Life prediction by maximum principal strain

From the nonlinear analyses, results of the three-dimensional finite element model are used to predict the fatigue lives. Here, the maximum principal strain is extracted to predict the fatigue life by using the following equation. (See section 2.3.1):

$$\frac{\Delta \varepsilon_1}{2} = \frac{\sigma_f'}{E}(2N)^b + \varepsilon_f'(2N)^c \tag{3.2}$$

Calculated maximum principal strains, predicted fatigue lives, and experimental cycles are shown in Table 3.3. Predicted cycles versus experimental cycles are depicted in Fig. 3.10.

Table 3.3 Predicted Fatigue Life Cycles Based on Maximum Principal Strain Criterion

Pure Bending			
Moment (N.m)	Percentage Strain	Predicted Cycles	Experimental Cycles
1460	0.22078	127887	382000
1475	0.2404	89264	354500
1708	0.27177	54597	92459
1730	0.27595	51450	49200
1875	0.30965	33307	43540
2586	0.51509	6023	5235
2600	0.51983	5853	5676
2800	0.58916	4002	2571
T/B=0.7			
Moment (N.m)	Percentage Strain	Predicted Cycles	Experimental Cycles
1250	0.2111	155449	325000
2550	0.28358	46349	97500
1720	0.35176	21076	21450
2325	0.56111	4634	3000
T/B=1.4			
Moment (N.m)	Percentage Strain	Predicted Cycles	Experimental Cycles
990	0.21699	137805	716382
1220	0.29765	38575	72000
1850	0.65122	2976	2045
T/B=1.9			
Moment (N.m)	Percentage Strain	Predicted Cycles	Experimental Cycles
1355	0.5194	5871	5500
T/B=2.8			
Moment (N.m)	Percentage Strain	Predicted Cycles	Experimental Cycles
845	0.25017	75864	200000
780	0.23548	97275	70681
1150	0.52422	5704	3000
T/B=3.6			
Moment (N.m)	Percentage Strain	Predicted Cycles	Experimental Cycles
570	0.28424	45919	80287
851	0.46656	8219	10000
Pure Torsion			
Torque (N.m)	Percentage Strain	Predicted Cycles	Experimental Cycles
2000	0.19414	226974	700000
2400	0.27514	52046	75700
2534	0.30737	34237	14331
3000	0.45721	8768	6329

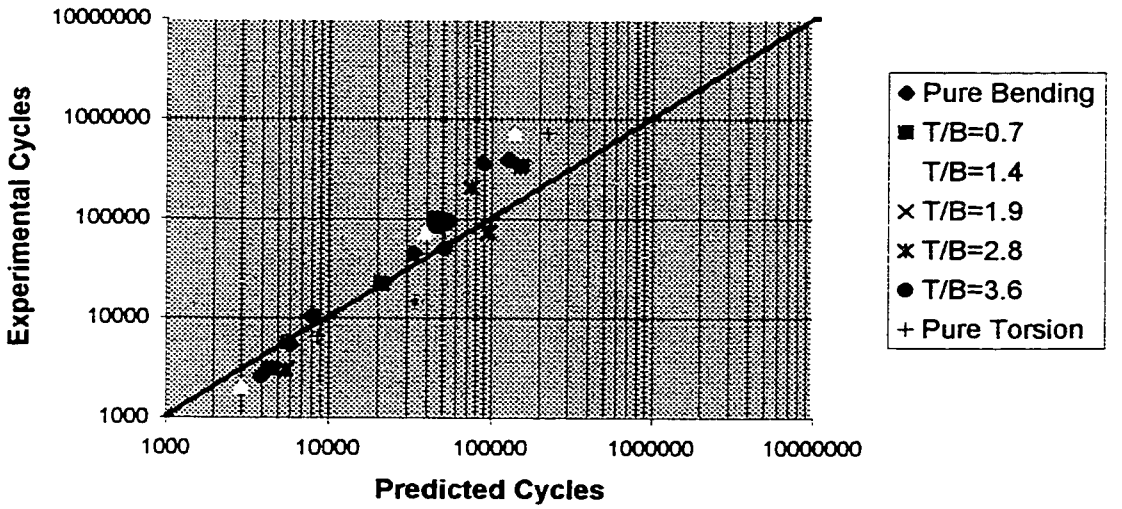

Figure 3.10 Experimental fatigue life cycles versus predicted fatigue life cycles (maximum principal strain criterion).

3.3.3 Life Prediction by maximum shear strain

The maximum principal strains for different type of loading are obtained from the three-dimensional finite elements analysis. Once this damaging parameter is at hand, the fatigue life is predicted by using the following equation. (See section 2.3.2):

$$\frac{\Delta\gamma_{max}}{2} = 1.3\frac{\sigma_f'}{E}(2N)^b + 1.5\varepsilon_f'(2N)^c \tag{3.3}$$

Calculated maximum shear strain, predicted fatigue lives, and experimental fatigue lives are shown in Table 3.4. Experimental fatigue cycles versus predicted fatigue cycles are depicted in Fig. 3.11

Table 3.4 Predicted Fatigue Life Cycles Based on Maximum Shear Strain Criterion

Pure Bending			
Moment (N.m)	Percentage Strain	Predicted Cycles	Experimental Cycles
1460	0.33903	81694	382000
1475	0.34466	76639	354500
1708	0.42735	34648	92459
1730	0.43433	32726	49200
1875	0.4918	21357	43540
2586	0.85604	3831	5235
2600	0.86446	3725	5676
2800	0.98956	2537	2571
T/B=0.7			
Moment (N.m)	Percentage Strain	Predicted Cycles	Experimental Cycles
1250	0.30996	116652	325000
2550	0.42751	34603	97500
1720	0.5608	13868	21450
2325	0.89219	3402	3000
T/B=1.4			
Moment (N.m)	Percentage Strain	Predicted Cycles	Experimental Cycles
990	0.30002	133294	716382
1220	0.41864	37274	72000
1850	0.95387	2813	2045
T/B=1.9			
Moment (N.m)	Percentage Strain	Predicted Cycles	Experimental Cycles
1355	0.76886	5244	5500
T/B=2.8			
Moment (N.m)	Percentage Strain	Predicted Cycles	Experimental Cycles
845	0.37633	54926	200000
780	0.35797	66286	70681
1150	0.8085	4523	3000
T/B=3.6			
Moment (N.m)	Percentage Strain	Predicted Cycles	Experimental Cycles
570	0.47839	23446	80287
851	0.76982	5225	10000
Pure Torsion			
Torque (N.m)	Percentage Strain	Predicted Cycles	Experimental Cycles
2000	0.38754	49281	700000
2400	0.54923	14834	75700
2534	0.61399	10398	14331
3000	0.91266	3189	6329

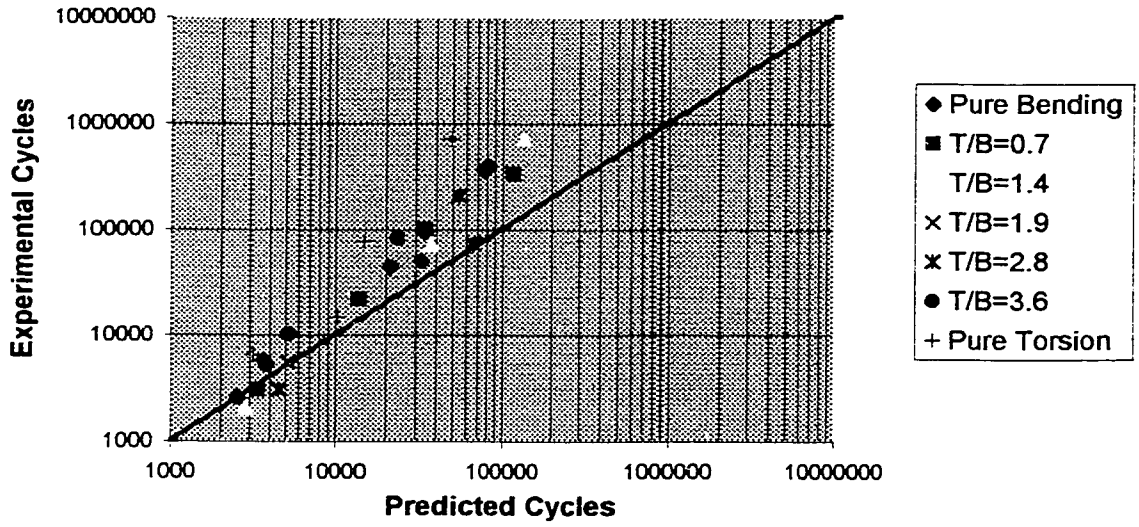

Figure 3.11 Experimental fatigue life cycles versus predicted life fatigue cycles (maximum shear strain).

3.3.4 General comparisons and discussions of fatigue life criteria

It is clear from Figs. 3.9 and 3.10 that the relationships between the experimental and numerical predictions do not follow the 45^0 straight line. However, the results show that the maximum principal strain delivers better correlation than the maximum shear strain. Moreover, the maximum shear strain is more conservative than the maximum principal strain, especially in high-cycle fatigue regions and torsion tests. Although, these two criteria show some agreement in low-cycle fatigue regions, these two approaches show a great difference in predicting the fatigue lives, and therefore cannot be considered as two identical methods that predict crack initiations.

This disagreement between the maximum principal strain and maximum shear strain motivates us to search for another approach that can be used as a unified method to predict the fatigue lives for low-cycle and high-cycle fatigue and more importantly, to estimate when the crack initiations occur.

3.4 Proposed approach based on energy density.

3.4.1 Introduction

The basic premise of this proposed methodology is that the fatigue crack starts to initiate at the critical location where maximum energy density is observed. This premise agrees with the fact that the area within the stable hysteresis loop represents the energy per unit volume Fig. (2.13).

The total strain energy per unit volume at the critical location, the notch, can be obtained from the three-dimensional finite element model. The objective is to obtain an equivalent uniaxial strain from the total strain energy density that is obtained from multiaxial stress-strain analysis. In other words, we are seeking an equivalent uniaxial strain that causes the same energy density in the uniaxial case.

Two approaches are investigated, one in which the energy density is obtained by elastic analysis, and the other is that the energy density is obtained by elastic -plastic analysis.

3.4.2 Fatigue life prediction by energy density based on elastic stress-strain field

It was shown by Hutchinson [8] for cracks, and by Walker [8] for deep notches, that in the case of localized plastic yielding the energy density distribution in the plastic zone is almost the same as linear elastic material. This means that, in the presence of localized small–scale plastic yielding, the gross linear elastic behavior of the material surrounding the notch controls the deformations in the plastic zone. Thus, it can be concluded that the energy density U_σ due to the local elastic-plastic stress-strain field is approximately equal to the strain energy density U_S due to elastic stress-strain field [8]:

$$U_S = U_\sigma \text{ or } \int_0^{e_{ij}} S_{ij}\, de_{ij} = \int_0^{\varepsilon_{ij}} \sigma_{ij}\, d\varepsilon_{ij} \qquad (3.4)$$

Where S_{ij} is local elastic stress tensor

σ_{ij} is the local elastic-plastic stress tensor

e_{ij} is local elastic strain tensor

ε_{ij} is local elastic-plastic strain tensor

In this methodology a three-dimensional elastic analysis of the finite element model is conducted and the strain energy density at the most critical location is determined by summing the contributions of all stress-strain components.

This calculated strain energy, U, is used to determine an equivalent uniaxial strain corresponding to energy density that is composed of elastic and plastic components in the uniaxial case. In other words, the strain energy density value obtained from three-dimensional finite element analysis is equated to a uniaxial energy density that is composed of elastic and plastic strain energies Fig.3.12. The mathematical formulation of this methodology is presented below.

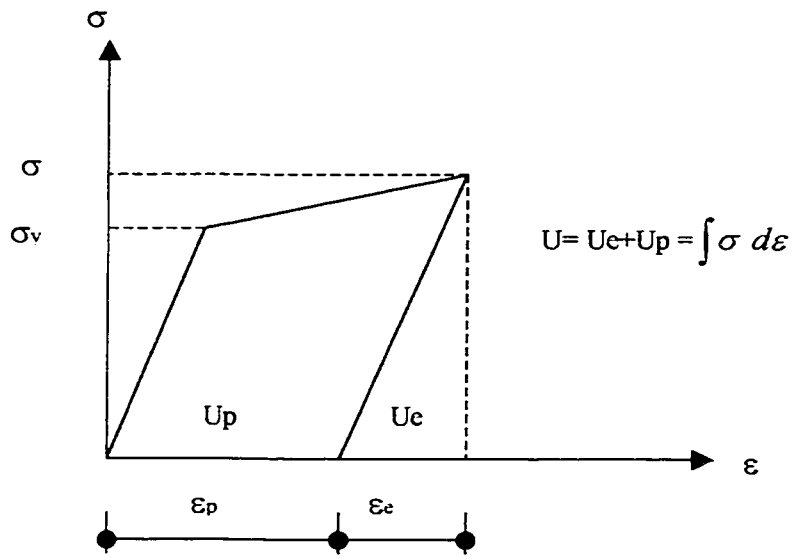

(a)

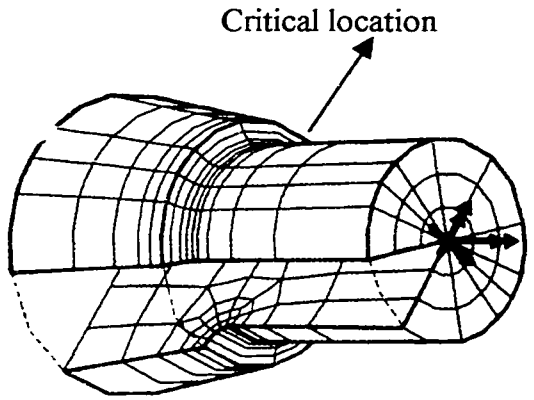

(b)

Figure 3.12 (a) A schematic representation of uniaxial stress-strain curve, (b) strain energy density can be obtained at critical location.

The total uniaxial strain energy per unit volume, energy density, can be obtained by integrating the area under the curve:

$$U = U_e + U_p = \int_0^{\varepsilon} \sigma \, d\varepsilon \tag{3.5}$$

We know that $\varepsilon = \frac{\sigma}{E} + (\frac{\sigma}{K'})^{\frac{1}{n'}}$ (3.6)

Therefore, $\frac{d\varepsilon}{d\sigma} = \frac{1}{E} + \frac{\sigma^{(\frac{1-n'}{n'})}}{n' K'^{\frac{1}{n'}}}$

Hence Eq. 3.5 becomes $U = \int \sigma \left(\frac{1}{E} + \frac{\sigma^{\frac{1-n'}{n'}}}{n' K'^{\frac{1}{n'}}} \right) d\sigma$

Therefore, $U = \frac{\sigma^2}{2E} + \frac{\sigma}{n'+1} (\frac{\sigma}{K'})^{\frac{1}{n'}}$ (3.7)

Solving Eq. 3.7, one can obtain the stress that is required to produce the same energy density in the uniaxial case. Back substituting the stress in Eq. 3.6, the corresponding strain is obtained.

Having the strain or the strain amplitude at hand, the fatigue life can be predicted by using the Manson-Coffin Equation.

$$\frac{\Delta \varepsilon}{2} = \frac{\sigma_f'}{E} (2N)^b + \varepsilon_f' (2N)^c \tag{3.8}$$

The perdicted lives using this methodology and the experimental fatigue lives given in reference [13] are presented in Table 3.5 and Fig 3.13.

Table 3.5 Predicted Fatigue Life Based on Multiaxial Elastic Strain Energy Density

Pure Bending			
Moment (N.m)	Percentage Strain	Predicted Cycles	Experimental Cycles
1460	0.1834	296592	382000
1475	0.186	277328	354500
1708	0.2221	127315	92459
1730	0.2256	116539	49200
1875	0.2493	76961	43540
2586	0.3782	16414	5235
2600	0.3809	16022	5676
2800	0.4209	11468	2571
T/B=0.7			
Moment (N.m)	Percentage Strain	Predicted Cycles	Experimental Cycles
1250	0.1731	392913	325000
2550	0.2242	119686	97500
1720	0.2626	62465	21450
2325	0.3483	21827	3000
T/B=1.4			
Moment (N.m)	Percentage Strain	Predicted Cycles	Experimental Cycles
990	0.1712	415039	716382
1220	0.2198	130367	72000
1850	0.3707	17583	2045
T/B=1.9			
Moment (N.m)	Percentage Strain	Predicted Cycles	Experimental Cycles
1355	0.3083	33855	5500
T/B=2.8			
Moment (N.m)	Percentage Strain	Predicted Cycles	Experimental Cycles
845	0.1984	205421	200000
780	0.2189	132656	70681
1150	0.3025	36335	3000
T/B=3.6			
Moment (N.m)	Percentage Strain	Predicted Cycles	Experimental Cycles
570	0.2057	174522	80287
851	0.2776	50306	10000
Pure Torsion			
Torque (N.m)	Percentage Strain	Predicted Cycles	Experimental Cycles
2000	0.1717	408935	700000
2400	0.2135	147914	75700
2534	0.2283	110816	14331
3000	0.2822	47207	6329

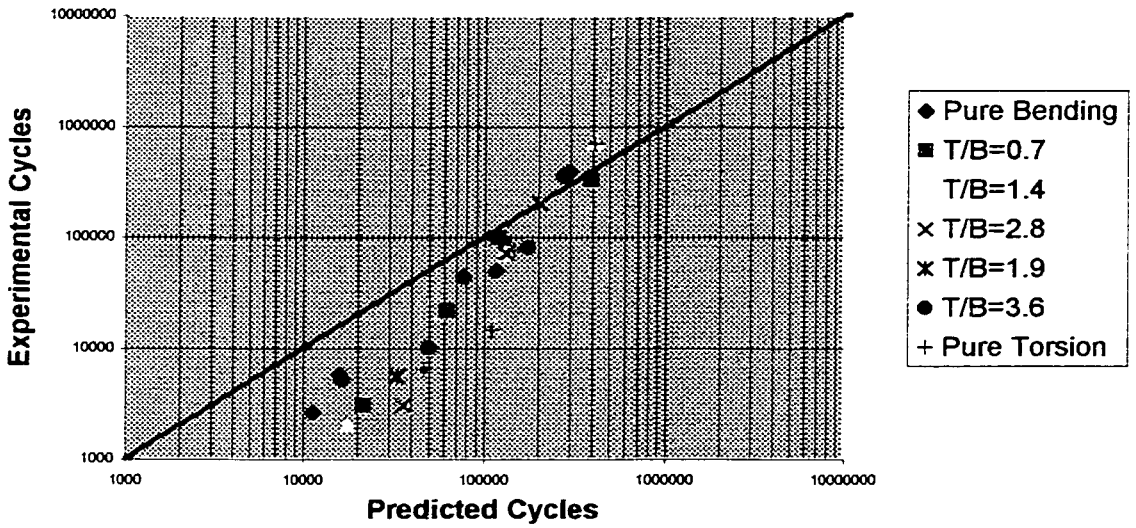

Figure 3.13 Experimental fatigue life cycles versus predicted fatigue life cycles (multiaxial elastic strain energy density criterion)

3.4.3 General discussion of fatigue lives predicted by enegry desnsity based on elastic stress-strain field

It is clear that this methodology delivres better results in high cycle fatigue region than the other two criteria that were tested in previous sections, specifically the maximum principal strain and maximum shear strain. However, this methodology overstimates the fatigue lives in low cycle fatigue region due to the fact that plastic strain is not accounted for properly.

It is worthwihle to remember that the basic premise of this methodology is based on the fact that the plastic strain is a small fraction of the total strain. That is why this methodology delivers the best estimates in high-cycle fatigue regions where the elastic strain controls the fatigue damage process.

It is obvious that this methodology does not serve as a unified tool that engineers can rely on in their daily practice, and therefore, this criterion failed to provide a unique approach that can be used for both high-cycle and low-cycle fatigue life predictions.

3.4.4 Fatigue life prediction by energy density based on elastic-plastic stress-strain field

In this methodology, an inealstic analysis of the three-dimensional finite element model is conducted and the energy density, U, (elastic and plastic) at the most critical location is predicted by taking into consideration contributions from all stress-strain components.

$$U = \int_0^{\varepsilon_{ij}} \sigma_{ij} d\varepsilon_{ij} \tag{3.9}$$

It is important to note that the strain energy densities for different loadings are easily obtained from ABAQUS data files. The obtained energy density value is, then used to define an equivalent uniaxial strain as explained previously for the elastic energy methodology in section 3.4.3.

The equivalent uniaxial strain is then used to predict the fatigue lives. Therefore, there is no difference of obtaining the equivalent strain, and hence, the fatigue lives between this methodology and the previous methodology except in that the strain energy calculations are based on elatic-plastic stress-strain field and elastic stress-strain field analysis respectively.

The predicted lives using this methodology and the experimental fatigue lives given in reference [13] are presented in Table 3.6 and Fig 3.14.

Table 3.6 Predicted Fatigue Life Cycles Based on Multiaxial Elastic-Plastic Strain Energy Density

Pure Bending			
Moment (N.m)	Percentage Strain	Predicted Cycles	Experimental Cycles
1460	0.1963	215721	382000
1475	0.199	202560	354500
1708	0.2423	86402	92459
1730	0.2466	80585	49200
1875	0.2766	50997	43540
2586	0.4615	8511	5235
2600	0.4659	8255	5676
2800	0.5298	5522	2571
T/B=0.7			
Moment (N.m)	Percentage Strain	Predicted Cycles	Experimental Cycles
1250	0.1861	276565	325000
1550	0.2506	75340	97500
1720	0.3089	33617	21450
2325	0.4937	6872	3000
T/B=1.4			
Moment (N.m)	Percentage Strain	Predicted Cycles	Experimental Cycles
990	0.1904	248527	716382
1220	0.2607	64277	72000
1850	0.5702	4414	2045
T/B=1.9			
Moment (N.m)	Percentage Strain	Predicted Cycles	Experimental Cycles
1355	0.462	8482	5500
T/B=2.8			
Moment (N.m)	Percentage Strain	Predicted Cycles	Experimental Cycles
845	0.2255	116730	200000
780	0.213	105428	70681
1150	0.4751	7760	3000
T/B=3.6			
Moment (N.m)	Percentage Strain	Predicted Cycles	Experimental Cycles
570	0.2701	55932	80287
851	0.4344	10682	10000
Pure Torsion			
Torque (N.m)	Percentage Strain	Predicted Cycles	Experimental Cycles
2000	0.214	146389	700000
2400	0.3006	37193	75700
2534	0.3375	24391	14331
3000	0.4972	6723	6329

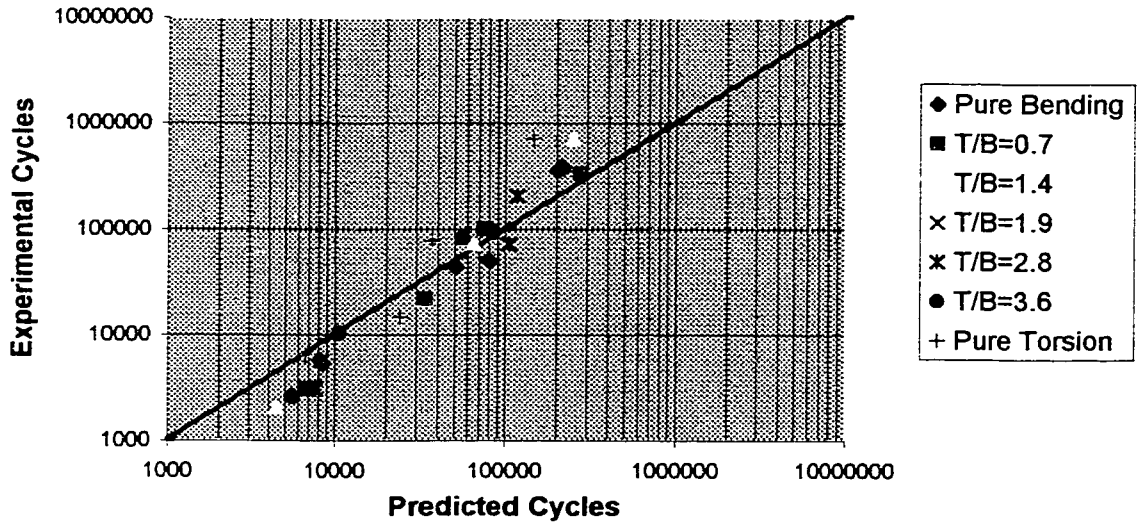

Figure 3.14 Experimental fatigue life cycles versus predicted fatigue life cycles (multiaxial elastic-plastic strain energy density criterion).

3.4.5 General discussion of fatigue lives predicted by enegry density based on elastic-plastic stress-strain field.

Visual comparison among Figs. 3.10 (maximum principal strain criterion), 3.11(maximum shear strain criterion), 3.13 (elastic strain energy criterion) and 3.14 (elastic-plastic strain energy criterion) shows that the overall correlation between experimental and predicted results in the entire range of low-to-high cycle fatigue , is best obtained with the elastic-plastic strain energy criterion.

It should be noted that the strain energy densities for this criterion are obtained at the integration points. Unfortunately, the strain energy densities are not obtained at the nodal points which are closer to surface where crack starts to initiate, this is due to fact that ABAQUS does not support this type of output; it only provides for this type of request at the integration points.

This methodology which is based on strain energy criterion that is calculated by elastic-plastic stress-strain field delivers better results than the other strain energy density approach which calculated by elastic stress-strain field . This improvement in life prediction is due to the fact that the plastic strain is accurately accounted for by conducting an elastic-plastic analysis.

3.5 Statistical and simple data analyses of fatigue lives criteria with respect to experimental results

In order to enable a quantitive comparsions among the fatigue lives criteria, statistical evalution of the ratios, between experimental and analytical fatigue lives is carried out. However, full statistical analysis for this type of data is not applicable, since the relationship between the predicted fatigue lives and the experimental fatigue lives is not dependent. In other words, there exists no such dependent variable and independent variable to describe a mathematical relationship so that a linear regression analysis can be performed.

Consequently, the mean, standard deviation, and the coefficient of variation are calculated for each fatigue life criterion so that one has an idea how the calculated data varies around its own mean. Also, another measure of dispersion of the ratio predicted to actual is the standard deviation around the optimum value one which indicates how well each fatigue life criterion varies around the perfect correlation.

Table 3.7 Statistical Data of the Ratio Between Analytical and Experimental Fatigue Lives

Criterion	Mean	Standard Deviation	Coefficient of Variation	Standard Deviation Around one	Maximum	Minimum
Max Principal Strain	0.932	0.561	60.2 %	0.565	2.39	0.192
Max shear Strain	0.596	0.379	63.7%	0.561	1.51	0.070
Strain Energy Density (elastic) N.mm/mm^3	3.49	3.06	87.9%	3.98	12.1	0.579
Strain Energy Density (Elastic-plastic) N.mm/mm^3	1.217	0.649	53.3%	0.685	2.58	0.209

In order to make relative comparisons among the fatigue lives criteria with respect to the experimental data, difference of fatigue lives for each fatigue life criterion is performed.

The experimental data are sorted in the ascending order so that one can distinguish how well each fatigue life criterion behaves in high-cycle and low-cycle fatigue regions. The difference is then calculated for each fatigue life criterion with respect to corresponding experimental value that is reported in the literature [12].

The relative difference, relative to experimental data, is defined as

$$\text{Re}\,\textit{lative difference} = (\textit{Experimental} - \text{Pr}\,\textit{edicted})$$

Tables 3.8 through 3.11 show the relative difference with respect to the experimental results. Fig 3.15 depicts experimental versus analytical results for cycles up to 10^5 . Fig 3.16 depicts experimental versus analytical results for cycles higher than 10^5 cycles.

Table 3.8 Difference in Cycles for Maximum Principal Strain Criterion

Experimental cycles	Predicted Cycles	Difference
2045	2976	-931
2571	4002	-1431
3000	4634	-1634
3000	5704	-2704
5235	6023	-788
5500	5871	-371
5676	5853	-177
6329	8768	-2439
10000	8219	1781
14331	21076	-6745
21450	21076	374
43540	33307	10233
49200	51450	-2250
70681	97275	-26594
72000	38575	33425
75700	52046	23654
80287	45919	34368
92459	54597	37862
97500	46349	51151
200000	75864	124136
325000	155449	169551
354500	89264	265236
382000	127887	254113
700000	226974	473026
716382	137805	578577

Table 3.9 Difference in Cycles for Maximum Shear Strain Criterion

Experimental Cycles	Predicted Cycles	Difference
2045	2813	-768
2571	2537	34
3000	3402	-402
3000	4523	-1523
5235	3831	1404
5500	5244	256
5676	3725	1951
6329	3189	3140
10000	5225	4775
14331	10398	3933
21450	13868	7582
43540	21357	22183
49200	32726	16474
70681	66286	4395
72000	37274	34726
75700	14834	60866
80287	23446	56841
92459	34648	57811
97500	34603	62897
200000	54926	145074
325000	116652	208348
354500	76639	277861
382000	81694	300306
700000	492821	207179
716382	133294	583088

Table 3.10 Difference in Cycles for Elastic Strain Energy Criterion

Experimental Cycles	Predicted Cycles	Difference
2045	17583	-15538
2571	11466	-8895
3000	21827	-18827
3000	36335	-33335
5235	16414	-11179
5500	33855	-28355
5676	16022	-10346
6329	47207	-40878
10000	50306	-40306
14331	110816	-96485
21450	62465	-41015
43540	76961	-33421
49200	116539	-67339
70681	132656	-61975
72000	130367	-58367
75700	147914	-72214
80287	174522	-94235
92459	127315	-34856
97500	119686	-22186
200000	205421	-5421
325000	392913	-67913
354500	277328	77172
382000	296592	85408
700000	408935	291065
716382	415039	301343

Table 3.11 Difference in Cycles for Elastic-plastic Strain Energy Criterion

Experimental Cycles	Predicted Cycles	Difference
2045	4414	-2369
2571	5522	-2951
3000	6872	-3872
3000	7760	-4760
5235	8511	-3276
5500	8482	-2982
5676	8255	-2579
6329	6723	-394
10000	10682	-682
14331	24391	-10060
21450	33617	-12167
43540	50997	-7457
49200	80585	-31385
70681	105428	-34747
72000	64277	7723
75700	37193	38507
80287	55932	24355
92459	86402	6057
97500	75340	22160
200000	116730	83270
325000	276565	48435
354500	202560	151940
382000	215721	166279
700000	146389	553611
716382	248527	467855

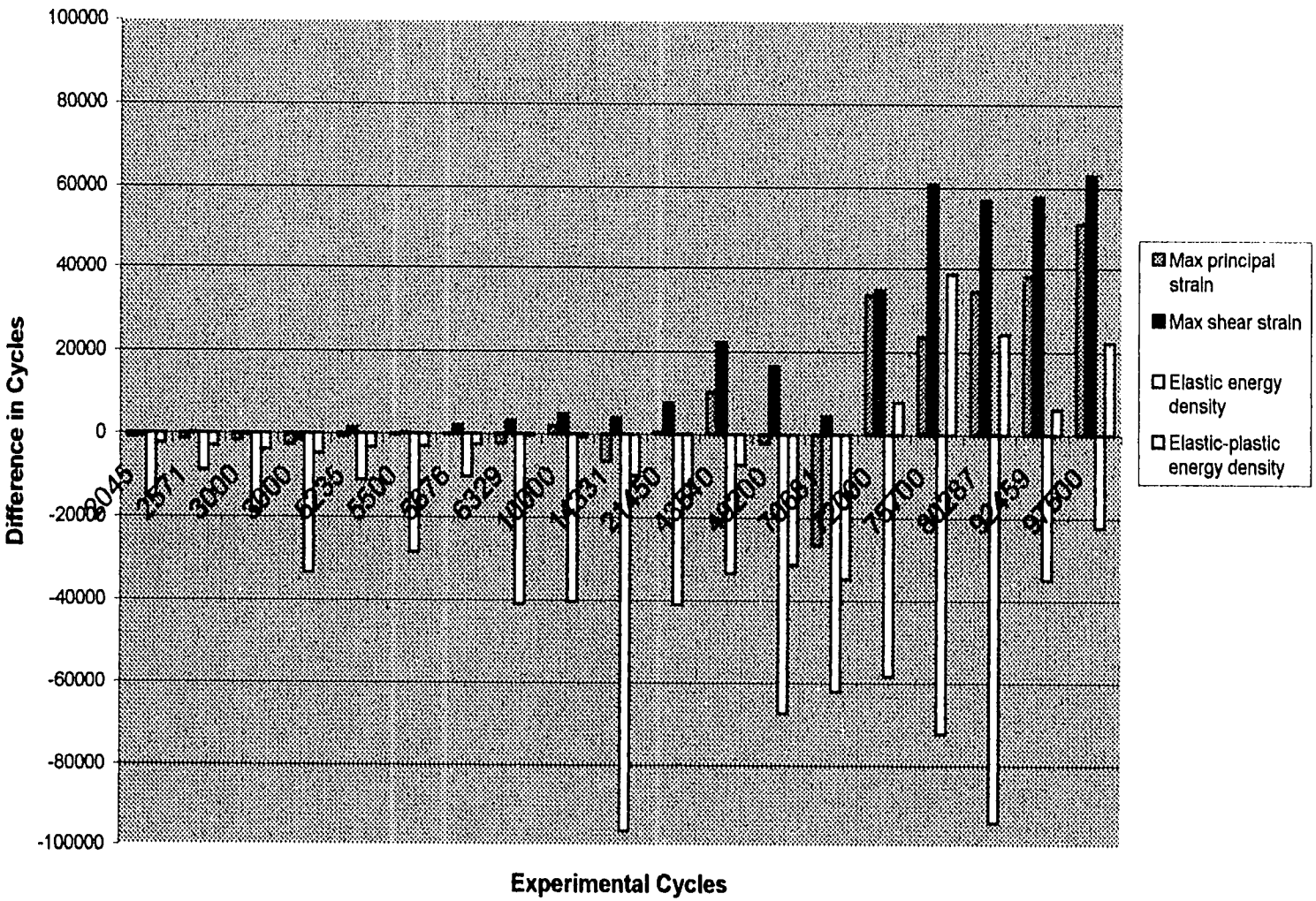

Figure 3.15 Experimental cycles versus difference in cycles between experimental and analytical results ($0\text{-}10^5$ range)

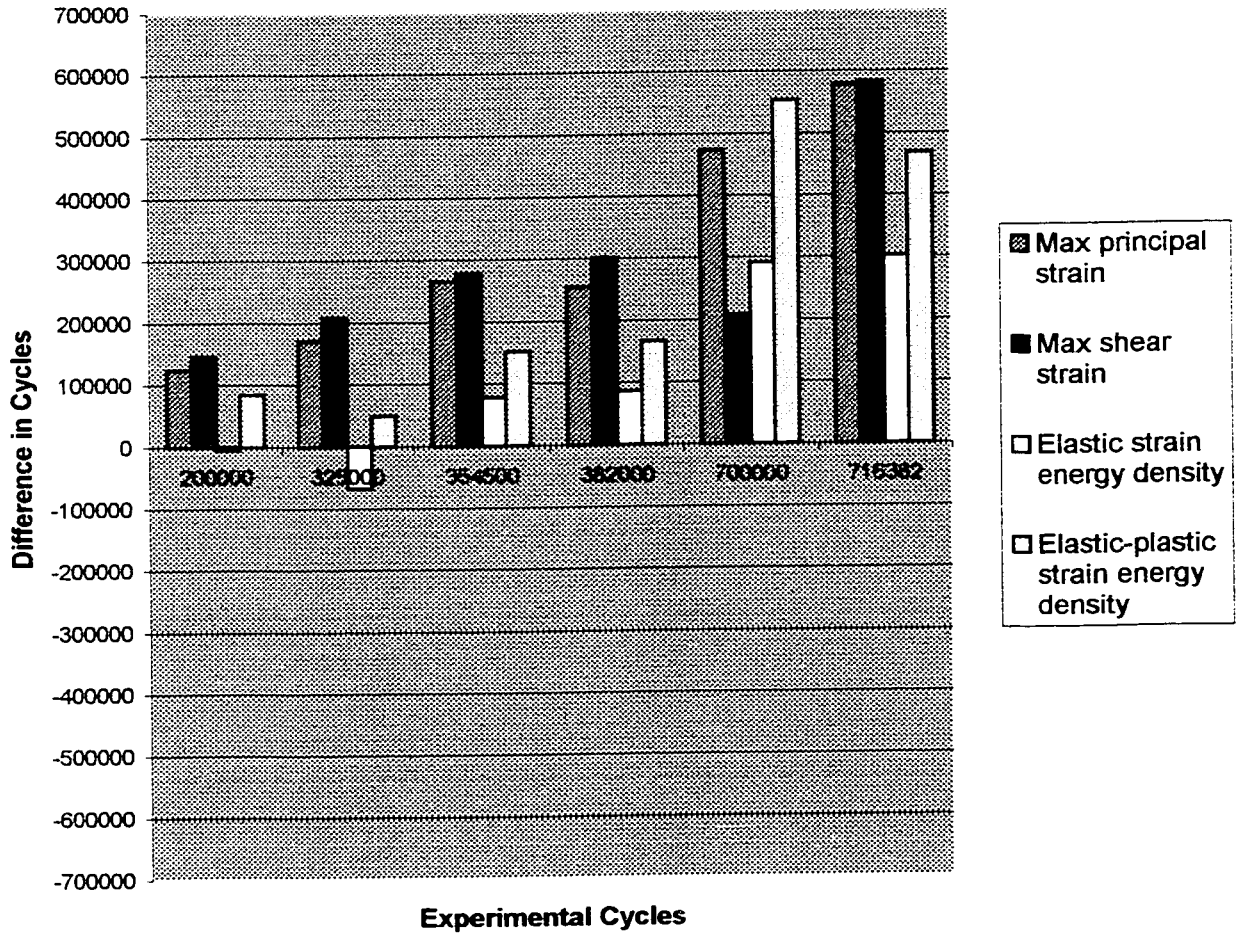

Figure 3.16 Experimental cycles versus difference in cycles between experimental and analytical results (10^5 and higher range)

3.6 Comprhensive discussion of fatigue lives criteria

Experimental fatigue lives versus estimated fatigue lives of the SAE notched shaft, have been shown in previous sections. Perfect correlation would lie along the 45^0 lines. Fatigue life comparisons, based on graphical observations and data analyses show that the maximum principal strain delivers the best results in low-cycle fatigue regions, however the results deviates significantly from the experimental results in high cycle-fatigue regions.

Although the maximum shear strain criterion delivers good results in low-cycle fatigue region (few cases), it is very conservative in predicting the fatigue lives. This is especially noticeable in torsion tests.

It is clear from the graphical comparisons and the simple data analyses that the energy density criterion based on elastic stress-strain field is only useful for high-cycle fatigue life prediction. This approach overestimates the fatigue lives in low-cycle fatigue drastically. Therefore this methodology failed to serve as a unified method that can be used for both low-cycle and high-cycle fatigue life predictions.

Finally, fatigue life predictions that are based on an elastic-plastic energy density criterion show equally good trend in low-cycle and high-cycle domains. This methodology delivers better results than the maximum principal strain criterion in high-cycle fatigue regions; the results of the low-cycle lives are also equally good. It can be said that this methodology predicts the fatigue lives consistently. It is believed that this methodology can be used for low-cycle and high-cycle fatigue problems.

It can be seen from the previous discussions that the choice of selecting a criterion to predict the fatigue crack initiation depends upon the fatigue domain. If the interested crack initiation falls in low-cycle fatigue domain the choice of using the maximum principal strain criterion would deliver a closer answer, with respect to experimental or

actual results, than the other fatigue lives criterion. However, if the interested crack initiation falls in high-cycle domain where elastic strain dominates the deformation, a choice of using the elastic strain energy density criterion would deliver a better answer than the other criteria. Consequently, the elastic strain energy density criterion is used to predict the fatigue crack initiation of two connecting rods where high-cycle fatigue is of our interest (see Chapter 4).

Although, the maximum principal strain and the elastic strain energy criteria serve as good damaging parameters to predict the fatigue crack initiation for low-cycle and high-cycle fatigue respectively, the elastic-plastic strain energy criterion can be used equally to predict fatigue crack initiations in high-cycle and low-cycle regions respectively.

Chapter 4
Industrial Application

4.1 Introduction

The objective in this chapter is to predict the fatigue crack initiation of two automotive connecting rods. Elastic strain energy density criterion, which has been found to be the best criterion, to predict fatigue crack initiation in high-cycle fatigue regions is employed to estimate the fatigue crack initiation of the two connecting rods.

Three-dimensional finite element analyses are performed on the two different connecting rods. The calculated stress-strain response parameters are, then, used to predict the fatigue crack initiation.

4.2 Problem description

Mascotech, an American automotive supplier company, has performed experimental fatigue life predictions on two of their connecting rods that are made from the same material. The two rods are similar in shape, but have different cross-sectional areas, specifically at the lower portion of the rod that connect the boreholes Figs 4.1 and 4.2.

In their experimental fatigue life predictions, Mascotech has used the same nominal stress on the two connecting rods and expected the fatigue lives of the two different connecting rods to be the same. However, experimental results showed that the two connecting rods have different fatigue life cycles. Consequently, the difference in fatigue lives motivated the company to pursue finite element analyses so that experimental conclusions are confirmed.

Figure 4.1 Finite element mesh of 2354 connecting rod

Figure 4.2 Finite element mesh of 2383 connecting rod

4.3 Finite element analyses

Three-dimensional finite element analyses were conducted on the two connecting rods. The 8-node brick elements and the wedge elements had been used in the analyses.

Elastic finite element analyses had been conducted on the two connecting rods. The elastic analyses showed that the applied load did not cause the material to yield. Consequently a high-cycle fatigue life was expected for both connecting rods.

For simplicity, the loads were applied on each connecting rod as two different cases, one in which the load is in tension Fig 4.3, and the other in which the load is in compression Fig. 4.4.

The damaging parameters, such as the maximum principal strains and strain energy densities, may have different amplitudes under tensile and compressive load cases. The difference in amplitude may occur due to the fact that the stress flow in the rod may differ with the nature of the applied force. Finite element analyses have shown that the tensile and compressive load cases have delivered the same amplitudes for the maximum principal strains and strain energy densities respectively. This similarity in amplitudes is due to the fact that stress distribution becomes uniform (Saint-Venant's principle) at the critical cross-section (Figs4.3 and 4.4), which is away from the applied load.

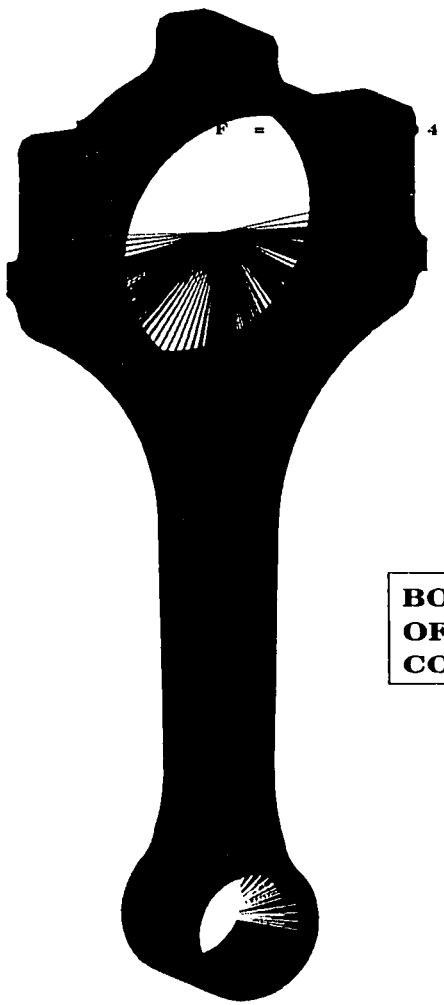

BOUNDARY CONDITIONS
OF 2354 CONNECTING ROD
COMPRESSION CASE

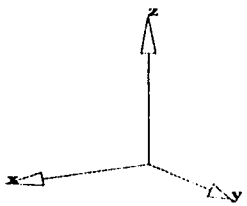

Figure 4.3 Compression load case of 2354 connecting rod

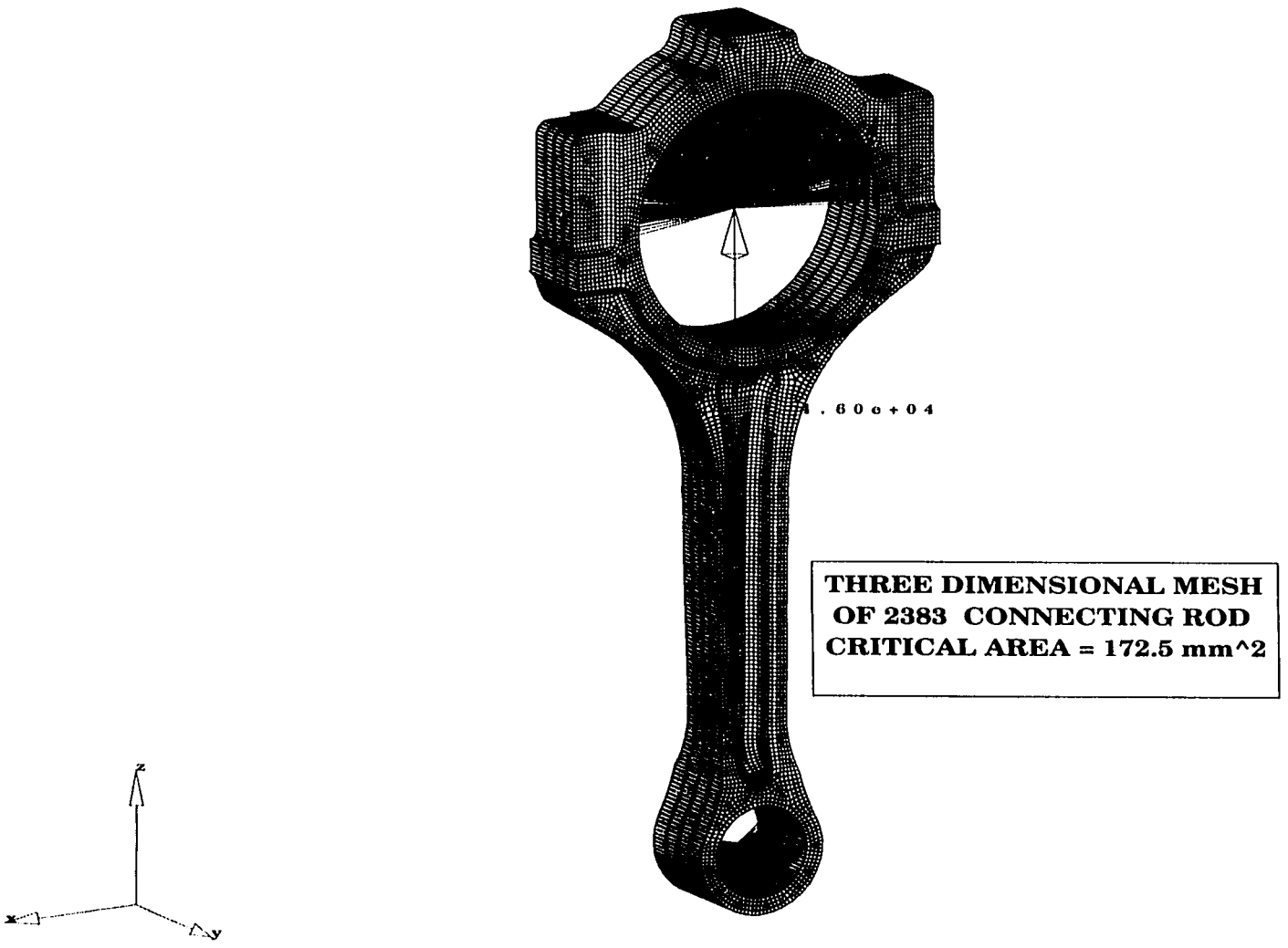

Figure 4.4 Tension load case of 2383 connecting rod

The objective is to operate the two connecting rods under the same nominal stress, 262 MPa (38 ksi), therefore the applied loads on both connecting rods varied according to their nominal cross-sectional areas. Table (4.1) shows the applied loads along with the obtained damaging parameters.

Table 4.1 Applied Loads and Corresponding Damaging Parameters

Rod ID	Nominal area (mm^2)	Nominal stress (MPa)	Applied load (N)	Max Principal strain (mm/mm)	Strain energy density ($N.mm/mm^3$)
2383 (tension)	172.5	262	45206	0.001560	0.2394
2383 (compression)	172.5	262	45206 N	- 0.001560	0.2394
2354 (tension)	167.2	262	43813 N	0.001984	0.3873
2354 (compression)	167.2	262	43813 N	- 0.001984	0.3873

4.4 Fatigue life predictions of connecting rods

4.4.1 Introduction

Based on the finite element analyses, the Von-Mises stresses are well below the yield stress; hence plastic strains do not exist and the deformation is controlled by the elastic strain. Consequently, high-cycle fatigue lives are expected for both connecting rods. Since, it was concluded that the strain energy density approach based on elastic stress-strain field delivers the best results for high-cycle fatigue life predictions, this approach is used to predict the fatigue lives of the two connecting rods.

4.4.2 Fatigue properties

It was shown in Section 2.3 that the total strain amplitude is related to the number of fatigue life cycles through Manson-coffin equation. In order to predict the fatigue lives, fatigue properties such as fatigue ductility exponent c, fatigue ductility coefficient ε_f', fatigue strength exponent b and fatigue strength coefficient σ_f' are needed to use the following equation:

$$\frac{\Delta\varepsilon}{2} = \frac{\sigma_f'}{E}(2N)^b + \varepsilon_f'(2N)^c \tag{4.1}$$

The material properties, read in Eq (4.1), are not known directly. However, the industrial sponsor (mascotech) had provided a cyclic stress-strain curve from which the stress and the plastic strain data have been extracted manually Fig.4.5.

These data when plotted on a log-log scale graph represent a near-straight line relationship Fig.4.6. The deviation from perfect straight line may be attributed to the error in manual extracting of data from the industry provided curve. Nonetheless, a best-fit line has been drawn through the data points. The slope of this line gives the material strain hardening exponent, n', and the stress ordinate corresponding to 100 % plastic strain has been taken as the strength coefficient K'.

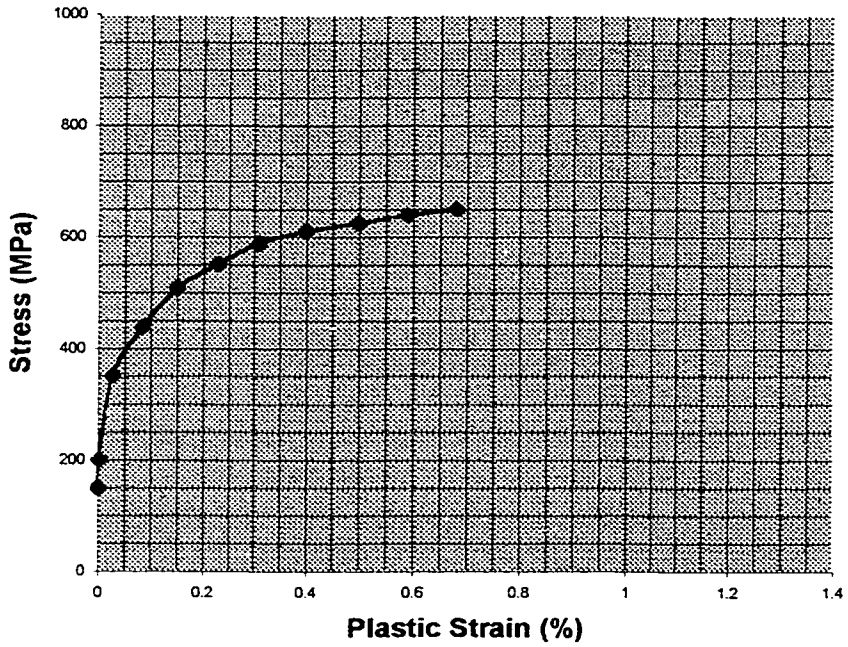

Figure 4.5 Stress plastic-strain relationship for connecting rod powder metal.

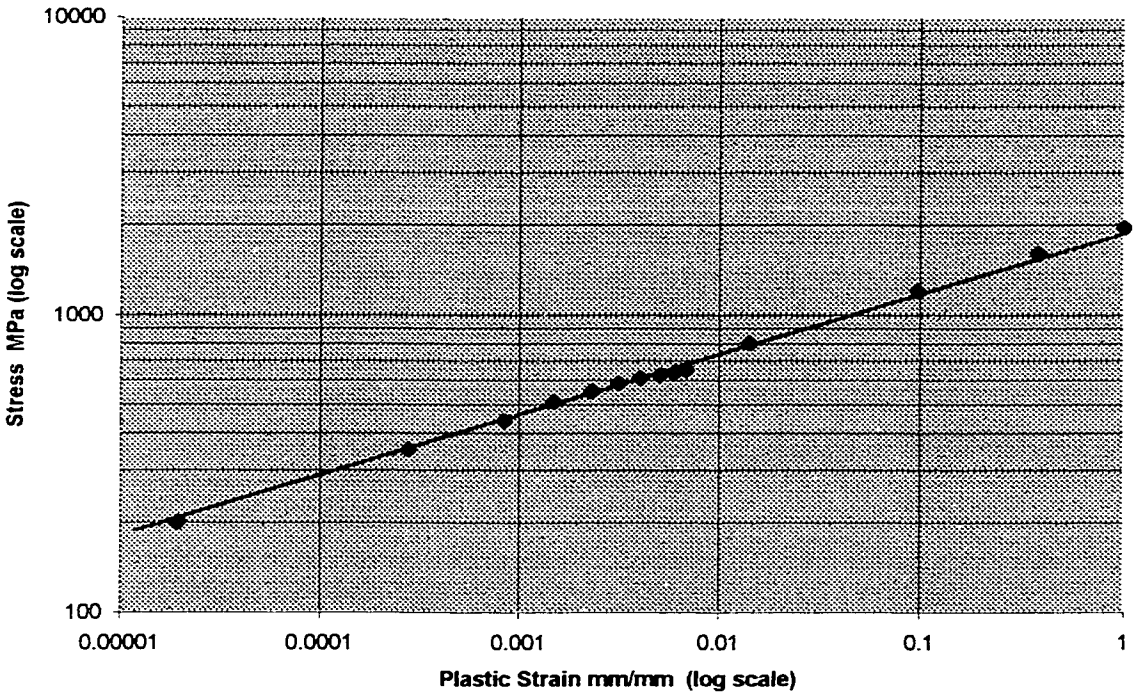

Figure 4.6 A log-log scale of plastic strain versus corresponding stress

The cyclic hardening exponent, n', is found to be 0.210 and the cyclic strength coefficient, K', is 1958 MPa. It should be noted that the parameters K' and n' depend on the available data that were read from the cyclic stress-strain curve. It is believed that the parameter K' is higher than expected. However, for the relative comparison between the 2383 and 2354 connecting rods the parameter K' would produce the same error in predicting the fatigue lives.

Once the material properties K' and n' are established, the fatigue properties (Eq. 4.2) are calculated by using the approach that proposed by Morrow [10]. Morrow has shown through an energy argument that b is related to the cyclic strain hardening n' as follows:

$$b = \frac{-n'}{(1+5n')} \tag{4.2}$$

For n'=0.21, we obtain b = - 0.102.

The fatigue ductility exponent is related to the strain hardening and the strength exponents as follows [12]:

$$n' = \frac{b}{c} \tag{4.3}$$

this gives, c = - 0.488

Finally, the last two requirements that are needed to predict the fatigue lives are the fatigue ductility coefficient ε'_f and the fatigue strength coefficient σ'_f. The cyclic strength coefficient K' is related to fatigue ductility and strength coefficients as follows:

$$K' = \frac{\sigma'_f}{\varepsilon_f'^{n'}} \tag{4.4}$$

Knowing that $\varepsilon'_f = \ln\frac{1}{1-RA} = 0.276$ (section 2.5.2.1), where RA= 24.14% provided by Mascotech, and substituting the values of K', n' and ε'_f in (Eq. 4.4) we obtain $\sigma'_f = 1494$ MPa. The derived parameters are summarized in Table (4.2).

Table 4.2 Uniaxial Fatigue Constants of the Connecting Rods

σ'_f (MPa)	b	ε'_f	c	E (MPa)
1494	-0.102	0.276	-0.488	204000

4.4.3 Fatigue life estimates

The strain energy density, based on elastic stress-strain field is used to predict the fatigue crack initiation of the two connecting rods. It was shown that this approach delivers the best results in high-cycle fatigue regime (section 3.4.2).

The strain energy density is used to extract the required stress by using the following equation:

$$U = \frac{\sigma^2}{2E} + \frac{\sigma}{n'+1}\left(\frac{\sigma}{K'}\right)^{1/n'} \tag{4.5}$$

Back substituting the extracted stress in the following equation, the required strain is obtained,

$$\varepsilon = \frac{\sigma}{E} + \left(\frac{\sigma}{K'}\right)^{\frac{1}{n'}} \tag{4.6}$$

The strain, equivalent to strain amplitude, is substituted in Manson-Coffin equation (Eq.4.1), and the fatigue crack initiation lives are estimated. The results are presented in Table 4.3.

Table 4.3 Damage parameters and Corresponding Number of Cycles

Rods ID	Energy Density (N.mm/mm^3)	Calculated Strain	Number of Cycles
2383	0.2394	0.001550	4,315,185
2354	0.3873	0.001998	740,813

4.5 Conclusions and recommendations

The analyses have shown that the two connecting rods have different fatigue crack initiation lives. The 2383-rod, whose cross-sectional area is greater than the 2354-rod, has longer fatigue life crack initiation. The obtained results showed that the 2383-rod fatigue life is about six times greater than the 2354-rod life. Therefore, based on the analyses, provided and extracted material properties that were used in the finite element analyses and fatigue life predictions, it can be concluded that the two connecting rods have different fatigue lives even though they were operated at the same stress level.

In order to predict the fatigue lives accurately, material properties should be provided as digital data so that solid conclusions could be made regarding the predicted fatigue lives. However, it is believed that the relative comparison between the connecting rods is valid to show the difference in fatigue crack initiations since the same material properties were used for both connecting rods.

Chapter 5
SUMMARY, CONCLUSIONS & RECOMMENDATIONS For FUTURE RESEARCH

5.1 Summary

Elastic and elastic-plastic three dimensional finite element analyses were conducted on the SAE notch shaft for different bending, torsion and combined bending-torsion loadings. The calculated stress-strain fields were used to predict the fatigue lives. The relative performance of two existing multiaxial fatigue theories, specifically, the maximum principal strain and the maximum shear strain criteria have been investigated. Two additional criteria based on the strain energy densities were also investigated.

All fatigue life predictions were based on a uniaxial equation that relates the damage parameter to the number of cycles, (namely the Manson-Coffin equation). The obtained fatigue lives, calculated using different multiaxial fatigue criteria, were compared to experimental fatigue lives that are reported in the literature [13]. The best criterion for high-cycle fatigue life prediction, as identified through the comparative studies, was subsequently used to predict the fatigue crack initiation lives of two automotive connecting rods.

5.2 Conclusions and recommendations

The following conclusions can be drawn from the analysis:

- The maximum principal strain criterion delivers the best results in low-cycle fatigue region whereas it deviates more than other criteria in high-cycle fatigue regions. Therefore, it is the opinion of the author of this thesis that the maximum principal strain criterion cannot be used to predict fatigue crack initiations for both low-cycle and high-cycle fatigue. However, this criterion is recommended for fatigue crack initiation predictions in low-cycle regions, where plastic strains control the deformation.

- The maximum shear strain criterion predicts the fatigue lives conservatively. Although, this criterion shows some good prediction in low-cycle fatigue regions, it cannot be considered as a reliable approach to predict high cycle fatigue crack initiations.

- The strain energy density approach, which is based on elastic stress-strain field, delivers the worst results in low-cycle fatigue regions. However it gives the best estimate in high-cycle fatigue regions. It is recommended to use this approach to predict fatigue crack initiation in high-cycle fatigue regions where plastic strain is a small portion of the total strain, in another word where elastic strain controls the deformation. This recommendation is being advised due to the fact that the damaging parameter required for this criterion can be extracted by performing elastic analysis, which is favored by most industries.

- The strain energy density approach that is based on elastic-plastic stress-strain field seems to predict the fatigue crack initiations consistently. In other words, it predicts the fatigue lives in high-cycle and low-cycle regions within an acceptable

range of variation, that is the scatter of ranges from one load case to another does not vary greatly compared to the other multiaxial fatigue life criteria. Consequently, it is believed that this criterion can be used as unified approach that engineers can depend upon to predict fatigue crack initiations in high-cycle and low-cycle fatigue regions.

It seems that the only recommendation for future research is that the strain energy density approach can be improved further by calculating the energy densities at the nodal points which are located at the surface of the critical location where cracks start to initiate.

As for the industrial problem of connecting rods, the following recommendations are presented:

- Stress-strain data for metal powder should be provided digitally so that reliable fatigue properties are used for life predictions.
- Fatigue crack propagation may be used to calculate the total fatigue life of each connecting rod. It should be clear that the fatigue lives that this thesis provided are only the crack initiation portion of the total fatigue life.

REFERENCES

[1] Bathe, K. J., (1996). Finite Element Procedures, Prentice Hall, Upper Saddle River, New Jersy 07458, pp 759-765

[2] Brown, M. W., and Miller, K.J., (1982), "Low-cycle Fatigue and Life Prediction, ASTM STP 770, American Society for Testing and Material", Philadelphia, pp 482-499

[3] Bannantine, J., and Corner, J., and Handrock, J., (1990), "Fundamentals of Metals Fatigue Analysis", Prentice Hall, Englewood Cliffs, New Jersey 07632.

[4] Cook, R. D, Malkus, D., and Plesha, M., (1989). "Concepts and Applications of Finite Element Analysis". Third Edition, John Wiley & Sons, Newyork.

[5] Collins. J.A., (1981), "Failure of Materials in Mechanical Design", A Wiley-Interscience Publication, John Wiley & Sons.

[6] Draper, J., January (1999), "Modern Metal Fatigue Analysis", Abaqus Series

[7] Fash, J. W., Darell, F. S., and David, L. M., (1985), " Fatigue Life Estimates for Simple Notched Component Under Biaxial Loading," Multiaxial Fatigue, ASTM STP 853, K. J. Miller and M. W. Brown, Eds, American Society for Testing and Materials, Philadelphia, pp. 497-513.

[8] Glinka, G., (1985), "Energy Density Approach To Calculation of Inelastic Strain Stress Near Notches and Cracks"Engineering Fracture Mechanics, pp 485-508.

[9] Hibbbit, Karlson & Sorensen, Inc. Abaqus, Finite Element Commercial Software, Theory manual version 5.8

[10] Landrgraf, R.W. (1970), "The Resistance of Metals to Cyclic Deformation," Achievement of High Fatigue Resistance in Metals and Alloys, ASTM STP 467, American Society for Testing and Material, pp 3-36.

[11] Lohr, R. D., and Ellison, E. G., (1980)," Fatigue of Engineering Materials and Structures", Vol. 3, pp 1-17.

[12] Hoffmann, M., and Seeger, T., (1986). "Stress-Strain Analysis and Life predictions of a Notched Shaft Under Multiaxial Loading". FG Werkstoffmechanik, Technische Hochschule Darmstadt, F.R.G

[13] Shigley and Mischke (1989), "Mechanical Engineering Design", Fifth Edition. McGraw-Hill, Inc. New York

Vita Auctoris

Name: Hicham Hussein El-Hage

Place of Birth: Lebanon

Year of Birth: 1966

Education: University of Windsor, Windsor, Ontario, Canada.
1990-1994, B.A.SC. in Civil Engineering
University of Windsor, Windsor, Ontario, Canada.
1999-2000, M.A.SC. in Mechanical, Automotive and Materials Engineering